Research Article

Hussam H. Kadhum, Sumayah Ibraheem, Zainab Nizar Jawad, Zuhair Mohammed Ali Jeddoa, Khetam H. Rasool, Majid S. Jabir*, Mazin A. Najm, Sabrean F. Jawad, Hayder M. Al-kuraishy, Uday M. Nayef, Ahmed Mutanabbi Abdula, Suresh Ghotekar, and Ayman A. Swelum*

Potential pharmaceutical applications and molecular docking study for green fabricated ZnO nanoparticles mediated *Raphanus sativus*: *In vitro* and *in vivo* study

https://doi.org/10.1515/ntrev-2024-0113 received May 9, 2024; accepted October 6, 2024

Abstract: The use of plant extracts as potent reducing agents for the environmentally friendly production of nanoparticles (NPs) has recently attracted the interest of scientists. NPs have received high attention because of

* Corresponding author: Majid S. Jabir, Department of Applied Sciences, University of Technology, Baghdad, Iraq, e-mail: 100131@uotechnology.edu.iq

* Corresponding author: Ayman A. Swelum, Department of Animal Production, College of Food and Agriculture Science, King Saud University, Riyadh, Saudi Arabia, e-mail: aswelum@ksu.edu.sa Hussam H. Kadhum: Department of Pharmacy, Al-Farabi University College, Baghdad, Iraq, e-mail: Hussam.hadi@alfarabiuc.edu.iq Sumayah Ibraheem: Department of Microbiology, Al-Kindy College of Medicine, Baghdad, Iraq,

 $e\hbox{-}mail: sumayahibraheem@kmc.uobaghdad.edu.iq\\$

Zainab Nizar Jawad: Department of Biology, College of Education for Pure Sciences, University of Kerbala, Karbala, Iraq,

e-mail: Zainab.n@uokerbala.edu.iq

Zuhair Mohammed Ali Jeddoa: Department of Basic Sciences, College of Pharmacy, Al-Zahraa University for Women, Karbala, Iraq, e-mail: zuhair.jeddoa@alzahraa.edu.iq

Khetam H. Rasool: Department of Biology, College of Science, Mustansiriyah University, Baghdad, Iraq, e-mail: dr.khr@uomustansiriyah.edu.iq

Mazin A. Najm: Department of Pharmacy, Mazaya University College, Dhi Qar, Iraq, e-mail: mazinsajad@gmail.com

Sabrean F. Jawad: Department of Pharmacy, Al-Mustaqbal University College, 51001, Hillah, Babylon, Iraq,

e-mail: sabrean.f.Jawaad@uomus.edu.iq

Hayder M. Al-kuraishy: Department of Clinical Pharmacology and Medicine, College of Medicine, Mustansiriyah University, Baghdad, Iraq, e-mail: haydermutter@uomustansiriyah.edu.iq

Uday M. Nayef: Department of Applied Sciences, University of Technology, Baghdad, Iraq, e-mail: uday.nayef@uotechnology.edu.iq **Ahmed Mutanabbi Abdula:** Department of Chemistry, College of Science, Mustansiriyah University, Baghdad, Iraq, e-mail: ahm.chem@uomustansiriyah.edu.iq

their novel properties. The aim of the present study is to biosynthesize zinc oxide nanoparticles (ZnO NPs) using Raphanus sativus and study their effect as antibacterial, anticancer, antiviral, and antidiabetic, agents, NLRP3 inflammasome inhibitors, and inducers of phagocytosis and autophagy. The antibacterial, anticancer, and antiviral activities of ZnO NPs were investigated using different assays: well diffusion assay, MTT assay, reverse transcription polymerase chain reaction, reactive oxygen species generation, and apoptosis assay. Meanwhile, immunofluorescent assay, enzyme-linked immunosorbent assay, and flow cytometry were used for detection of autophagy and phagocytosis. Docking was also achieved to study their binding mode as well as affinity within the target enzymes (glucosamine-6-phosphate synthase) (PDB:1MOQ) active site, estrogen receptor (PDB:3ERT) active site, and tubulin receptor (PDB:402B) active site. The results demonstrated that the ZnO NPs have an inhibitory role against bacteria and the proliferation of lung cancer cells (A549). IC₅₀ was 22.78 μg/mL for A549 cells. For MCF-10, was 272.24 μg/mL, antiviral activity against influenza virus, and antidiabetic agent. Conversely, the results showed the ability of ZnO NPs to reduce inflammasome activity via induction of autophagy. The study's findings show that R. sativus can be easily and effectively used to synthesize ZnO NPs, and they also highlight the ZnO NPs' considerable potential as antibacterial, antiviral, anticancer, NLRP3 inflammasome inhibitor, antidiabetic agent, and phagocytosis and autophagy inducer. Based on our findings, the green synthesized ZnO NPs could be used as promising therapeutic agents for biomedical applications.

Suresh Ghotekar: Centre for Herbal Pharmacology and Environmental Sustainability, Chettinad Hospital and Research Institute, Chettinad Academy of Research and Education, Kelambakkam, 603103, Tamil Nadu, India, e-mail: ghotekarsuresh7@gmail.com

Keywords: ZnO NPs, antimicrobial, apoptosis, autophagy, inflammasome, molecular docking

1 Introduction

Nanotechnology is a hot spot research in recent material sciences, providing numerous applications ranging from innovative fabric compounds to sophisticated medical applications [1]. Nanotechnology involves synthesizing and exploring molecules ranging from 1 to 100 nm nanoscale. which correspond with the functional properties of anthropogenic systems [2]. Nanoparticles (NPs) are manipulated or controlled particles at the atomic level 1-100 nm with distinct physiochemical properties from bulk materials [3]. NPs are regarded as larger than their counterparts. NP drug delivery system has been used since the 1990s and has evolved alongside advanced technological needs to enhance the delivery of different therapeutics. Newer generations of NPs have been developed over the past few decades to improve novel therapeutic modalities [3]. These characteristics of NPs make them to be used in different spectra, including nanomedicine. NPs of metal oxide have important physiochemical and biological properties, making them valuable in different applications. In NP synthesis, many adverse effects develop due to toxic chemicals such as capping and reductive agents. However, using natural, mainly plant extracts in the synthesis of NPs is promising as it is eco-friendly and time-saving [3]. NPs have unique metal intrinsic properties such as zinc oxide (ZnO) and silver [4]. ZnO is a multipurpose and promising molecule with a wide range of applications [5] due to heat stability, long durability, high selectivity, and high optical absorption, which is essential for the detection of the antibacterial response [6]. ZnO NPs can be synthesized from different natural extracts. ZnO NPs have good biocompatibility than zinc metal in biological tissues. Zinc metal is highly present in different tissues, including skin, bone, brain, and muscles. Therefore, non-toxic ZnO NPs are highly distributed in the human body [6]. Different methods are used for the synthesis of ZnO NPs, e.g., spherical shape ZnO NPs are synthesized by hydrothermic method [7]. Specific features of NPs permit them to interact with numerous cell biomolecules and facilitate transport into the inner cellular components [8]. ZnO NPs have a higher atomic percentage and large surface reactivity. Therefore, it can interact with living organisms [9]. ZnO NPs can accumulate intracellularly, leading to the inhibition of the growth of bacterial and cancer cells due to their special physical and chemical characteristics, ZnO NPs are among the most studied options

among all NPs for drug delivery, cancer diagnostics, and therapeutic applications [10]. ZnO NPs are currently one of the five zinc compounds that the US Food and Drug Administration lists as usually considered safe for both animals and humans. ZnO was observed as one of the best metal NPs in the world since it is affordable, hygroscopic, nontoxic, and easily accessible. ZnO NPs are widely investigated in both nanoscale and microscale formulations for their antibacterial activity [11]. ZnO NPs exhibit bactericidal effects through interaction with bacterial cell walls or bacterial nucleic acids by releasing Zn²⁺ and generating reactive oxygen species (ROS) [12]. Fabrication of ZnO NPs with desirable shapes and sizes protects the human body from solar radiation and bacterial infections [13]. Moreover, selective toxicity of ZnO NPs could be beneficial against cancer cells [14]. Autophagy is a necessary process for normal homeostasis and the health of the skin [15]. The skin, which is made up of many cells and is the greatest barrier in the body, protects organisms from infections and regulates their metabolism and immune system to keep them in a state of dynamic balance. However, a number of issues impede the healing of skin wounds [16]. The healing of wounds is a very intricate biological process that encompasses multiple cell types working in harmony as well as joint involvement [17]. Inflammation, oxidative stress, and bacterial infections are examples of health issues that can hinder the healing of wounds and create excruciating agony for the patient. Furthermore, extended medical care strains the healthcare system and consumes enormous quantities of medical resources [18]. Autophagy is essential for skin repair because it encourages immunological and functional cells to help heal damaged skin more quickly. According to a study by Birmingham's group, resistance to pathogenic infections and autophagy activation are positively correlated. Additionally, Salmonella typhimurium can induce autophagy, which stops it from multiplying in cells and shields them from bacterial harm [19]. According to a study by Das et al., vitamin D increased macrophage autophagy, which in turn increased the expression of antiinflammatory proteins and decreased the inflammatory response, thereby accelerating skin healing [20]. It has been demonstrated that biomaterial-mediated autophagy is crucial for cell phagocytosis and clearance, cellular function maintenance, cell differentiation, and immunological stress in vitro and in vivo [21]. The incredibly intricate homeostatic mechanism of living things can stop the aberrant materials, such as protein clumps, from accumulating when breakdown processes are activated. As a result, biomaterials that enter the body are quickly identified as alien substances that trigger a number of cellular defense responses, such as autophagy [22]. Biomaterials have a

significant impact on how certain diseases proceed by controlling autophagy [23], through controlling autophagy during skin wound healing [24]. Clinicians are always faced with more complex wound healing cases; hence, new materials and methods are highly sought after. Significant advancements in nanotechnology, primarily in the areas of nanochemistry and nanomanufacturing, have completely transformed the biotechnology and pharmaceutical sectors. Because of their unique structures, nanomaterials (NMs) (having at least one dimension smaller than 100 nm) exhibit distinctive physicochemical features to surface, macroscopic, and small-scale quantum tunneling phenomena. Recently, because of their improved adsorption ability, antibacterial qualities, and medication loading, NPs are used in healing of wound [25]. Zinc oxide nanoparticles (ZnO NPs) are widely used in medicinal product fillers because of their antimicrobial, biosafety, and biocompatible capacity [26]. The cytoplasm and surface of the bacterial cell absorb and accumulate ZnO NPs, respectively, and impair the bacterial cell membrane, causing the bacterium to die. Previous research has indicated that the size of ZnO NPs is crucial in inhibiting the growth of some detrimental bacteria [27]. For instance, ZnO NPs are used as bactericidal factor [28]. Aqueous solution of ZnO NP has antibacterial action via induce a lot of ROS [29]. Additionally, it was found that direct contact and strong ROS production may greatly kill Mycobacterium using ZnO NPs. Moreover, ZnO NPs, in a dose-dependent manner, prevent the growth of P. aeruginosa and S. aureus biofilms. ZnO NPs embedded in cellulose sheets [30], collagen dressing [31], or chitosan hydrogel [32] demonstrated tissue regeneration as well as antibacterial action, making them appropriate for reducing the risk of infections during wound healing [33]. Many factors could affect NPs' biological activity, such as size distribution, shape, surface charge, surface chemistry, capping agents, and others. Researchers have been interested in NMs for the past few years due to their unique properties, such as physical, chemical, biological, and nanoscale, which set them apart from bulk materials [34]. A recently published study examined the use of NP-based formulations for colon cancer diagnostics and treatment [35]. Meanwhile, Rehman et al. [36] demonstrated that the Mn_{0.5}Zn_{0.5}Dy_xEu_xFe_{1.8-2x}O₄ NPs have antibacterial and anticancer potential roles. Nowadays, scientists are able to encapsulate medication in virus-sized NPs. Because the NPs can precisely locate damaged cells and transfer the medication, they are suitable for the system of drug delivery. Furthermore, advances in nanoscience and nanotechnology are driving the creation of increasingly advanced instruments for neurosurgery and early disease diagnosis, including cancer and atherosclerosis. The field of using nanotechnology to diagnose diseases is expanding quickly. These materials are outstanding and essential in many applications because of their special size-dependent characteristics [37]. Therefore, the aim of this study was to evaluate the biomedical applications of bio-synthesized ZnO NPs such as antimicrobial, anticancer, antioxidant, antidiabetic, phagocytosis induction, and targeting NLRP3 inflammasome via augment autophagy.

2 Materials and methods

2.1 Green synthesis of ZnO NPs

This experiment was done according to Liu et al. [38]. Briefly, 1 gm of R. sativus red root was stirred and heated at 80°C in 50 mL distilled water (DW) for 45 min; the pH of the extract was 7.3. Then, Whatman filter paper was used to filter the extract. After that, 2 mL of plant extract was added to 2 mL of 0.5 M of zinc acetate dehydrate for 45 min. The mixture was then centrifuged at 5,000 rpm for 30 min at 4°C. The mixture was stirred continuously while 2 M NaOH was added dropwise to create a white precipitate. After that, the reaction was completed by continuing to stir for 2 h. Centrifuging the mixture at 4,000 rpm produced the precipitate, which was then cleaned with DW until its pH reached 7.2. In order to create pure ZnO NPs, the precipitate was finally dried for 2 h at 80°C.

2.2 Characterization of NPs

The UV-vis absorbance of the NPs was determined by using a UV-1700 Shimadzu spectrophotometer and measuring the absorbance throughout a wavelength range of 200-800 nm. Scanning electron microscopy (SEM) and transmission electron microscopy (TEM) were used to study the morphological characteristics of the ZnO NPs. Finally, fourier transform infrared spectroscopy (FTIR) was used to determine the functional group of ZnO NPs [39-41].

2.3 Anticancer activity of ZnO NPs

2.3.1 MTT assay

The cytotoxicity assay of ZnO NPs was done. A549 (Passage No. 17) and MCF-10 (Passage No. 12) cells (Gift from the Iraqi Center for Cancer Research and Medical Genetics) were cultured at a density of 1×10^4 cells per well using complete RPMI-1640 tissue culture media. After 24 h, the cells were exposed to different concentrations of ZnO NPs for 72 h. MTT solution was added to the cells for 3 h at a concentration of 2 mg/mL. Then, 100 μ L of DMSO is added. At a wavelength of 492 nm, the absorbance of each sample was evaluated using a microplate reader [42–44].

2.3.2 Acridine orange/ethidium bromide (AO/EtBr) staining

A549 and MCF-10 were plated on 12-well plates at a density of 1×10^6 cells/well. After 24 h, ZnO NPs at IC₅₀ were added. Then, the cells were stained for 2 min with 10 µg/mL AO/EtBr. A fluorescence microscope was used to examine the cells [45].

2.3.3 Real-time PCR

This experiment was done to measure the expression of P53, BAX, BCL-2, P53, and mRNA using PCR. The sequences of primer sets used in this experiment within the quantitative RT-PCR assay involved: BAX (forward: 5'-ATGAAGCT GAGCGAGTGT-3' (reverse: 5'-AGCTGGGATGATCCTCTG-3'), BCL-2 (forward: 5'-CCTGCACAGCTGGATCCT) (reverse: 3'-GACAGAGCCAGCAGAAATCTAA), and P53 (forward'- CGG TCG CAA GCT ATG GAT G-3') (reverse: 5'-GAA GAT GAC ATT GGC CAG CAG-3'). DNase treatment was used after the cells' total RNA was extracted. On the other hand, Superscript II reverse transcriptase (Invitrogen) was used in the product in order to synthesize cDNA. The following ingredients were added to each reaction for the quantitative reverse transcription polymerase chain reaction (q RT-PCR): 1 µL cDNA, 7.5 µL SYBR green, 0.3 µL ROX, and 0.3 µL relevant primers. The final volume was increased to 15 μL by adding 5.6 μL of DW. Fast SYBR A 7900HT rapid system was used to apply the green master mix. Gene expression levels were normalized to TATA-binding protein, and then their mean relative values were computed using the established techniques (Livak and Schmittgen) [46].

2.4 Antibacterial activity of ZnO NPs

The well-diffusion method was used to measure the antibacterial activity of ZnO NPs against *S. pyogenes* and *P. aeruginosa*. The bacteria were cultured on the Mueller Hinton agar plates. Wells with diameters of about 6 mm were made at the surface of agar media. Then, ZnO NPs were added at different concentrations into the wells. These plates were kept in the incubator for 24 h. The antibacterial activity of ZnO NPs was recorded by measuring the inhibition zone

diameters. The viability of bacterial strains was investigated using AO/EtBr double staining assay [47,48]. SEM is used to investigate morphological changes in bacterial strains after being treated with ZnO NPs.

2.4.1 Crystal violet staining

ZnO NPs at 125 μ g/mL were applied to bacterial strains cultured in 24-well plates at a concentration of 1 × 10⁶ CFU/mL for a duration of 24 h. After three rinsing with DW, the samples were then stained with crystal violet (0.1%, Sigma) and cleaned with phosphate buffer saline (PBS). Crystal violet-stained samples were filled with 0.2 mL of 95% ethanol and agitated for 2 h to measure the growth of biofilms. Next at 595 nm, the optical density was measured.

2.4.2 Antibiofilm activity of ZnO NPs

Filmtracer Live/Dead Biofilm Viability Kit was used to stain biofilms that were grown on culture plates of Lysogeny broth medium (HiMedia, India) or left untreated (control) or treated with ZnO NPs at a concentration of 125 μ g/mL for 24 h. Using a Leica TCS SP5 II confocal microscope, the pictures were taken.

2.4.3 Biofilm metabolic activity investigation

In glass tubes, biofilms developed both bacterial strains in the absence and presence of ZnO NPs. Following a 48-h anaerobic incubation period at 37°C , the biofilm suspension was stained using a Live/Dead dye kit and subjected to flow cytometry analysis. In summary, the samples were washed twice by PBS and centrifuged at 2,000 rpm for 2 min. Syto 9 (30 μM) and propidium iodide (10 μM) were added for 10 min. When the sample containing two stain components was stimulated at 488 nm, the emission was recorded using the propidium iodide (670/LP) channel and the Syto 9 (530/30) channel on the fluorescein isothiocyanate (FITC) channel. The percentage of untreated control cells was used to express the biofilm cell viability data.

2.5 Antiviral activity of ZnO NPs

2.5.1 Hemagglutination inhibition (HAI) test

The test detects the capacity of ZnO NPs to inhibit the formation of hemagglutination caused by the H1N1 influenza A virus.

2.5.2 Embryonic inoculation assay

The HlNl virus sample was diluted with DW and ZnO NPs for 4 h in 1.5 mL Eppendorf tubes. Fertile chicken embryos that were 10 days old were individually injected with 100 µL of a sample that was obtained using the chorioallantoic sac method. After being injected for 72 h at 37°C, the eggs were refrigerated for 12 h at 4°C. As previously mentioned, the viral HAI titers of the chorioallantoic sac fluid were assessed.

2.5.3 Cytotoxicity assay

To determine the cytotoxicity of ZnO NPs against MDCK cells (Purchased from Sigma), the cells were cultured at a density of 1×10^4 cells per well. After 24 h, the cells were exposed to different concentrations of ZnO NPs for 3 h. MTT solution was added to the cells for 3 h at a concentration of 2 mg/mL. Then, 100 µL of DMSO was added. At a wavelength of 492 nm, the absorbance of each sample was evaluated using a microplate reader.

2.5.4 ZnO NPs inhibit viral neuraminidase

Using the commercial kit Neuraminidase Assay Kit MAK121, antiviral activity evaluation of ZnO NPs was carried out in MDCK cells infected with Influenza A (H1N1) and compared to Oseltamivir as positive experimental control.

2.5.5 Flow cytometry assay

To determine the ability of ZnO NPs as inhibitor of cell apoptosis when induced by the H1N1 influenza A virus, and to examine the MDCK cells' early apoptotic activity, a flow cytometry experiment was employed. There were three groups in this test. In the first group, MDCK cells were left untreated, in the second and third groups, viral control is applied to MDCK cells, and ZnO NPs are used to treat the virus for 3 h. After collecting, the cells were combined with RNase A, rinsed three times in ice-cold PBS, and incubated for 30 min at 37°C. After adding propidium iodide (PI) to the mixture, the samples were left in the dark for 30 min at 4°C. Finally, the binding buffer was added to the cells. The results were analyzed with a flow cytometry machine. The ROS level was monitored by analyzing the intensity of the ROS probe (DCFH-DA), which was incubated for 45 min in complete darkness. A flow cytometer was used to gather the cells and measure their fluorescence intensity (BD Biosciences).

2.6 Antioxidant activity of ZnO NPs

2.6.1 DPPH assay

In summary, a 2.4 mg methanolic DPPH solution was supplied. After that, 3.995 mL of the DPPH standard solution was combined with 5 µL of ZnO NPs at various concentrations (25, 50, 75, 100, and 125 µg/mL), and the mixture was incubated for an additional 20 min. The following equation was used to record the DPPH radical absorbance at 515 nm, and the COPD-NC radical scavenging activity was calculated.

Radical scavenging activity =
$$\frac{\text{Sample OD - Control OD}}{\text{Control OD}}$$
$$\times 100.$$

2.6.2 2,2-azino-bis(3-ethylbenzothiazoline-6-sulfonic acid (ABTS) activity

By supplying an ABTS solution with equal amounts of ABTS (7 mM) and potassium persulfate (2.45 mM) solutions, the activated radicals of ABTS were created. Following a 12 h dark incubation period at 25°C, the diluted ABTS standard solution was supplied, and the ABTS radical absorbance (0.7) at 734 nm was recorded. Finally, 3.995 mL of the ABTS standard solution was combined with 5 µL of the produced ZnO NPs at various concentrations (25, 50, 75, 100, and 125 µg/mL) and incubated for an additional 20 min. The absorbance of ABTS radicals at 734 nm was used to evaluate the radical scavenging activity of ZnO NPs.

2.7 Anti-diabetic activity of ZnO NPs

2.7.1 α-Amylase inhibition assay

About 0.5 mg/mL α-amylase was incubated with and without the sample for 10 min at 25°C. A pH 6.9 solution of sodium phosphate buffer (0.02 M) was prepared. Following dilution to a concentration of 100-300 µg/mL, the ZnO NP sample was mixed with the buffer solution and incubated for 10 min at 25°C. Following the previously indicated procedures, the buffer solution was mixed with 1% starch solution and incubated for 30 min. Dinitrosalicylic acid was added to halt the enzymatic reaction, and the mixture was subsequently heated to 100°C for 15 min in a water bath. At 540 nm, the absorbance was measured. A positive control was a solution containing acarbose. % α-Amylase inhibition = $[(A_0 - A_i/A_0)] \times 100$. A_i is the sample's absorbance, while A_0 is the absorbance of the control.

2.7.2 Animal model

Fifteen male mice were weighed at the start and had an average age of 8 weeks. Before the experiment started, all the animals were kept in one house for 5 days. Three groups of animals were randomly assigned; the first group was used as a control, and the second group consisted of five mice that received a single intraperitoneal dosage of streptozotocin (50 mg/kg) to induce diabetes. For 25 consecutive days, the third group – diabetic + ZnO NPs groups – received an oral daily dosage of ZnO NPs at a dose of 5 mg/kg.

2.7.3 Induction of experimental diabetes

The 100 mg/kg of streptozotocin (STZ) (Sigma Chemical Co., Poole, Dorset, UK) administered intraperitoneally once in 0.01 M sodium citrate buffer (pH = 4.5) was used to cause experimental diabetes mellitus. The rats were fed a diet heavy in fat and sugar (10% sucrose, 20% margarine, and 65.5% basal rat food). Freshly produced STZ was injected into 40 rats. Following an injection of stem cells, fasting blood glucose levels were measured. Rats exhibiting blood glucose levels greater than 250 mg/dL were classified as diabetic and placed in diabetic groups.

2.7.4 Sampling protocol

Every experimental mouse had a tail vein used to draw blood samples. After centrifugation, the serum (~150 μ L) was isolated and kept at –20°C for further analysis to determine the blood glucose levels. The liver tissues were extracted and then mixed to measure the amount of glucokinase (GK).

2.7.5 Biochemical determinations

The glucose oxidase method was used to estimate blood glucose levels (mg/dL). Blood glucose levels were assessed in all experimental animals before the start of the procedure and following injection of streptozotocin. Blood glucose levels were regularly monitored in animals with targeted-induced diabetes until diabetes was identified (animals with blood glucose levels greater than 250 mg/dL are considered diabetics). Subsequently, blood glucose levels were tracked for every experimental animal, and findings were acquired

at the conclusion of the trial. A rat insulin ELISA kit (Catalog No. ezrmi-13kelisa, EMD Millipore, Billerica, MA, USA) was used to quantify the serum insulin level and GK activity in liver tissue.

2.7.6 Histopathological examinations

Pancreatic specimens were gathered, preserved in 10% buffered neutral formalin solution, gradually dried out in 70–100% ethanol, cleaned in xylene, and embedded in paraffin. Hematoxylin and eosin (HE) dyes were regularly used to make 5 μ m thick paraffin sections, which were subsequently inspected under a microscope.

2.8 Induction of phagocytosis by ZnO NPs

2.8.1 Assessment of the phagocytic activity

Following their isolation, bone marrow-derived macrophages (BMDMs) were seeded in 6-well plates at a concentration of 4×10^5 . ZnO NPs were produced 24 h after cells were treated with *A. cepa* extract at a dose of 25 µg/mL. Methylene blue was used at a concentration of 0.5% to stain *Candida albicans* that had been cultured with BMDMs at a ratio of 1:5 for 60 min. The transparent cells were regarded as active, and the blue ones were inactive when the cells were counted and observed. The results were presented as an index of phagocytosis (PI).

2.8.2 Assay of phagosome/lysosome fusion

The BMDMs were separated and seeded at a density of 1×10^5 cells/mL in RPMI-1640 medium onto 4-well chamber slides. ZnO NPs were added to the BMDMs for 1h at a concentration of $25~\mu g/mL$ after 10 h. After loading the cells with 25 nM of Lysotracker Red for 60 min at 37°C, the cells were treated with *E. coli* conjugated with FITC at a multiplicity of 1:50 for 2 h. Lysotracker Red was added while the infection was active. The cells were washed five times in sterile, cold PBS before being fixed with 4% paraformal-dehyde. The samples were viewed under a fluorescent microscope (Olympus, Tokyo, Japan) after being mounted. Phagosomes that were not fused and contained FITC-bacteria showed up as green stain, while lysosomes that had Lysotracker labels showed up as red. Because of the merging

of the two labeled fluorochromes, the phagosome and lysosome fusion appeared to be yellow.

2.8.3 Phagocytosis of pHrodo E. coli bioparticles by **BMDMs**

In a 4-well plate, BMDMs were seeded with ZnO NPs at a concentration of 25 µg/mL as a pretreatment. After adding 100 µL of pHrodo-E. coli particles, they were incubated for 2 h with 100 µL of buffer solution added. Following cell fixation, the flow cytometry assay was performed to interpret the data.

2.9 ZnO NPs induce autophagy

2.9.1 Immunofluorescent assay

Seeding of BMDM cells was achieved onto plastic Lab-tek two-well slides. After that, the cells were either left untreated or treated with the produced lipopolysaccharide (LPS) for 12 h at a concentration of 500 µg/mL and 5 mM/mL of adinosine triphosphate (ATP) in the presence and absence of ZnO NPs at a concentration of 25 µg/mL. The cells were then following the standard protocol, which included three PBS washes, fixation with 4% PFA for 30 min at room temperature. Then, the samples were permeabilized by 0.5% Triton-X for 30 min at room temperature and blocked with 10% normal goat serum for 60 min. Primary and secondary antibodies were added following the standard protocol. Finally, a confocal microscope is used to visualize the results.

2.10 Anti-inflammation activity of ZnO NPs

2.10.1 Isolation of BMDMs

Primary BMDMs were isolated using male C57/BL6 mice that were 8-10 weeks old. Following their isolation, the BMDM cells were subjected to LPS for 12 h at concentrations of 500 µg/mL and ATP for 30 min at a concentration of 5 mM, in the presence and absence of ZnO NPs at a concentration of 25 µg/mL, to examine their capacity to decrease NLRP3 inflammasome activation and IL-1 secretion.

2.10.2 ELISA assay

Using an enzyme-linked immunosorbent assay (ELISA) kit, the cytokine concentration of mouse IL-1\beta and NLRP3 (Abcam, USA) was determined in accordance with the manufacturer's instructions. An ELISA plate reader set at 570 nm was used to measure the absorbance.

2.11 In silico study (molecular docking study)

The crystal structures of glucosamine-6-phosphate synthase (GlcN-6-P synthase [PDB code 1MOQ)), Estrogen receptor (PDB code 3ERT), and colchicine in complex with tubulin (PDB code: 402B) were obtained from RCSB PDB (RCSB PDB: Homepage). The substrate or the inhibitor inside the target enzyme or protein was removed, as well as water molecules and modified amino acids. The crystal structure of the macromolecules was processed by the Pyrx AutoDock Vina software (0.8). Three-dimensional structures of selected three active components from the red radish root were constructed using ChemDraw ultra 7.0 as mol file and converted into pdb format using Open Babel. The three compounds were then molecularly docked inside the binding. The determined dimensions were X = 32.02, Y = 16.58, Z = -2.64 with size equal to 27.01, 31.01, and 26.59 for the GlcN-6-P synthase, while the dimension applied for the RE alpha target were X = 29.59, Y = -0.20, and Z = 25.00 with size equal to 31.24, 27.04, and 28.90 as the grid spacing, respectively. The dimensions applied for the tubulin target were X = 18.36, Y = 64.81, and Z = 42.12, with sizes equal to 36.23, 35.24, and 32.05 as the grid spacing and the affinity (kcal/mol) value was calculated. We, however, used optimal interactions and the best Auto-Dock score for the interpretation of the best conformation. Finally, the results were visualized and analyzed using Discovery Studio 2021. The validity of docking protocols was confirmed via redocking of crystalized substrate or inhibitor within the target binding pocket. Redocking of the medication (colchicine), 4-HYD-ROXYTAMOXIFEN, and crystallized substrate (GlcN-6-P) within the binding pocket of the corresponding target verified the validity of the docking protocols.

2.12 Statistical analysis

For statistical analysis, we used an unpaired t-test on the collected data using Graph-Pad Prism 6. The data were represented as mean ± SD of triplicate permanents [49]. A one-way ANOVA test was used to determine the statistical significance levels *, **, and ***, which stand for p-values less than 0.05, 0.01, and 0.001, respectively.

Ethical approval: The Health Research Ethics Committee at the University of Technology (ASDUOT/13052022) had reviewed and deemed this study ethically feasible. Additionally, this study adhered to the Declaration of Helsinki's requirements.

3 Results

3.1 Characterization of ZnO NPs

A UV-1700 Shimadzu spectrophotometer characterized the ZnO NPs to determine the UV-vis absorbance of the NPs, as indicated in Figure 1a. SEM and TEM investigated the morphology of ZnO NPs as shown in Figure 1b and c. Finally, FTIR was used to determine the functional groups of prepared ZnO NPs data that were not shown.

3.2 Anticancer activity of ZnO NPs

The upper panel of Figure 2 represents the anticancer activity of ZnO NPs against lung cancer cells as well as normal cell lines. The results demonstrated that the ZnO NPs can inhibit the proliferation of cancer cell lines but not normal ones. The ability of ZnO NPs to destroy cancer cells is concentration-dependent. To investigate the ability of ZnO NPs on the reduction of cancer cell growth A549 lung cancer cell lines were treated with higher concentrations of ZnO NPs, as illustrated in Figure 2 (upper panel), the number of treated cancer cells was considerably decreased. The selective toxicity of ZnO NPs is indicated by the lower IC₅₀ concentration of the NPs for A549 cancer cells as compared to MCF-10 cells. AO/EtBr staining assays were performed to measure the viability of cancer and normal cell lines. For the AO/EtBr assay, A549 cells were exposed to ZnO NPs at IC50. The outcomes showed that the

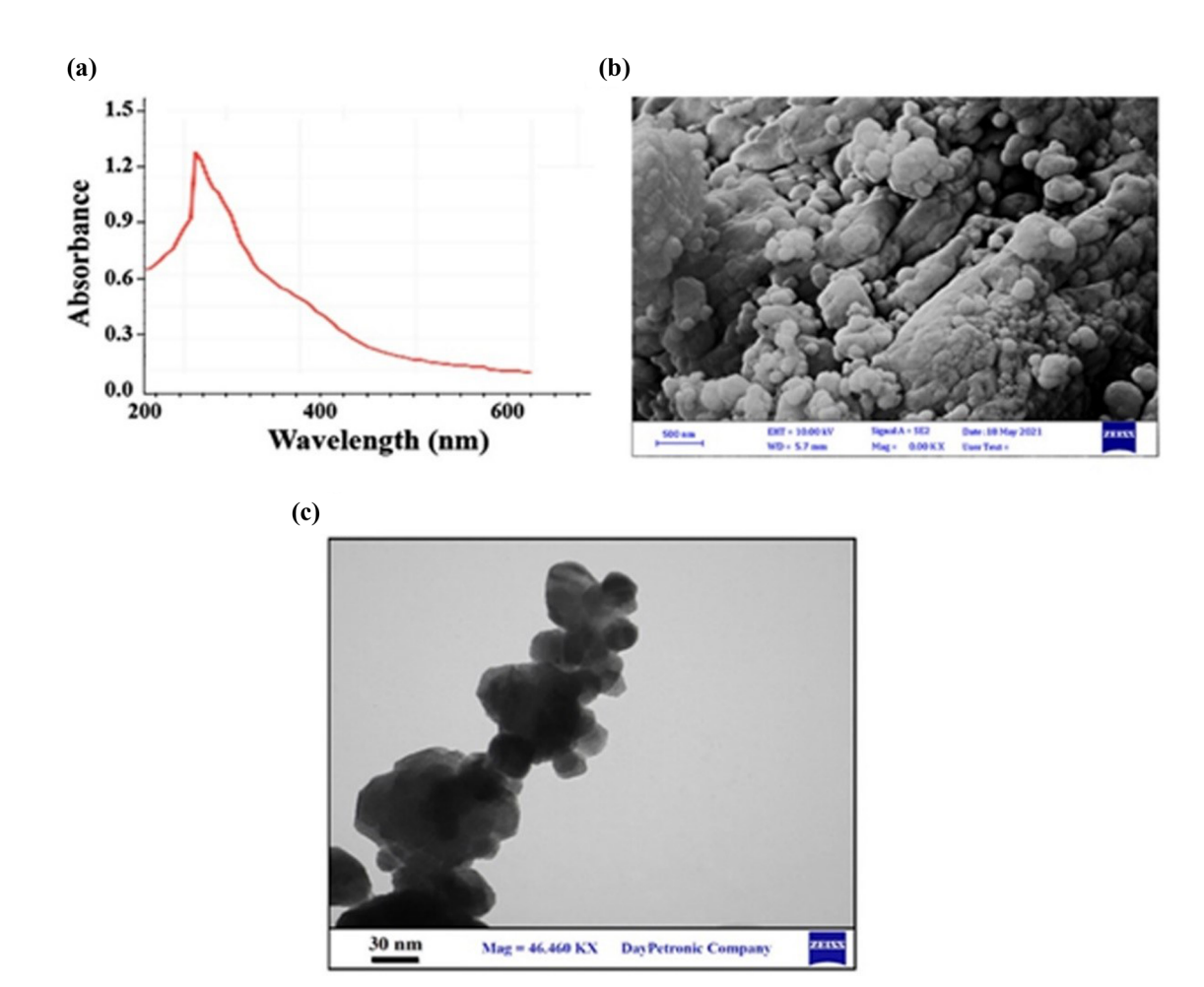


Figure 1: Characterization of ZnO NPs. (a) UV-spectra, (b) SEM image, and (c) TEM image.

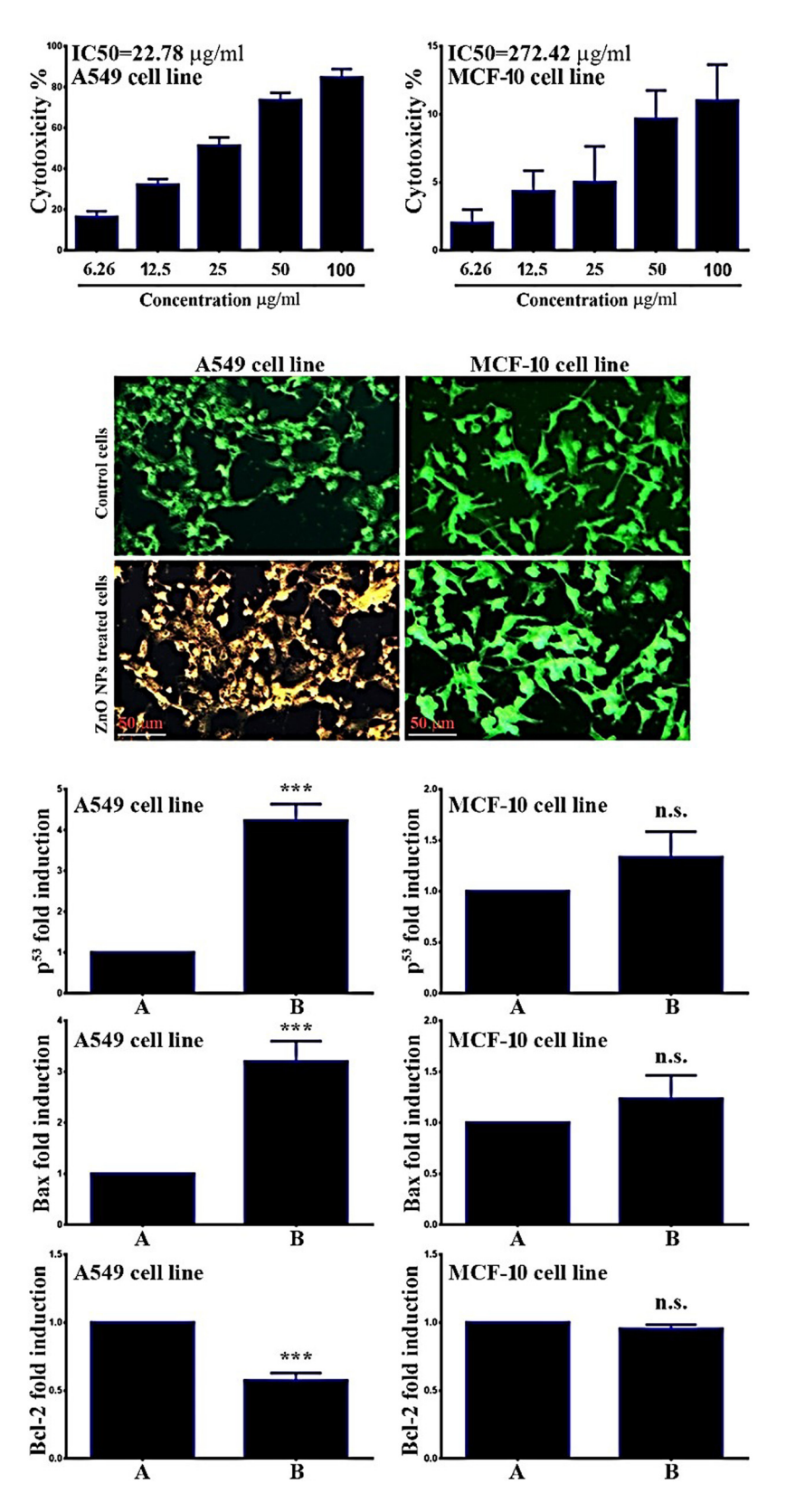


Figure 2: Anti-cancer activity of ZnO NPs against A549 lung cell lines. Upper panel shows MTT assay results. Middle panel shows AO/EtBr double staining assay. Lower panel shows RT-PCR results. The data were represented as the mean value ± standard deviation of three different experiments.

untreated control A549 cells were stained with AO (Green), indicating that they were living cells. As shown in Figure 2 (middle panel), the ZnO NP-treated cells were stained with EtBr, a yellow-orange dye that denotes dead cells. No changes were observed in the normal cell line after being treated with ZnO NPs. To study the ability of ZnO NPs in apoptosis gene expression, we investigated p53, BAX, and BCL-2 levels. The results showed the ability of prepared ZnO NPs to upregulate and downregulate the apoptosis proteins, as shown in the lower panel of Figure 2.

3.3 Antibacterial activity of ZnO NPs

In the present study, the antibacterial activity of ZnO NPs was evaluated against S. pyogenes, and P. aeruginosa. The zones of inhibition were measured and reported. Taken together, the inhibition zone of ZnO NPs is in a concentration-dependent manner, as shown in the upper panel of Figure 3. The mechanism of bacterial inhibition by ZnO NPs is dependent on multiple parameters and strongly affected by the size and the morphology of NPs, in addition to the kind of strain. Fluorescence microscopy was used to distinguish between live and dead bacterial strains using AO/EtBr double staining assay. AO is responsible for staining live cells. While EtBr was responsible for the staining of dead bacteria. For both bacterial strains, as in the middle panel of Figure 3, all untreated bacterial strains appeared green, and following treatment with ZnO NPs, the bacterial strains appeared orange-red. SEM was utilized to investigate how ZnO NPs affected the development and structure of bacterial strains. The lower panels of Figure 3 show the differences between the ZnO NPs treated bacteria and control samples. The results show that an untreated bacterial strain confirmed the cluster-form colonies. SEM images show that S. pyogenes and P. aeruginosa were destroyed by ZnO NP treatment, as shown in the lower panel of Figure 3. The synthesized NPs under study exhibit notable antimicrobial activity. Damaged colonies have an impact on the bacterial strain. After the cells were treated with the produced NPs, morphological alterations, osmotic imbalance, and the integrity of the cell structure were all induced by an osmotic imbalance that resulted in a leak of bacterial cells.

Figure 4 shows how ZnO NPs may prevent bacterial strains from forming biofilms. One crucial stage in the beginning of any infection was the creation of biofilms. One crucial first stage in the creation of biofilms is the adherence of bacterial strains to a surface, which can happen through both specialized and nonspecific cell-

surface interactions. The attached bacterial cells can be stained with crystal violet to identify these biofilms. Figure 4 (upper panel) illustrates how ZnO NPs inhibited the growth of biofilms in this study. Confocal microscopy was utilized to examine the impact of ZnO NPs on the suppression of bacterial biofilms. At 125 µg/mL, the antibiofilm activity of ZnO NPs was confirmed by the confocal microscope images. Based on membrane integrity, the biofilm viability kit's two-color fluorescent dye is utilized to identify living and dead bacterial cells within the biofilm community. Bacteria with intact cell membranes were stained fluorescent green, while those with damaged membranes were stained fluorescent red, as shown in Figure 4 (middle panel). The bacterial strains with damaged membranes were penetrated and stained with propidium iodide red fluorescence dye, while the membranes in good condition were stained by Syto 9 green fluorescence dye. Untreated control bacterial strains assembled and formed a developed biofilm layer; the ZnO NPs at concentration of 125 µg/mL had a less dense biofilm coating and were less aggregated. The findings of this investigation highlight the impacts of ZnO NPs, as well as their ability to prepare ZnO NPs to suppress biofilm formation. Using a flow cytometry technique, the biofilm metabolic activity of bacterial strains was examined. The dot plots of S. pyogenes and P. aeruginosa are displayed in Figure 4 (lower panel). In this study, flow cytometry using excitation/emission fluorescence Syto 9 and propidium iodide staining helped distinguish between live and dead cell populations. It measured the metabolic activity in the S. pyogenes and P. aeruginosa biofilms formed over 48 h. As illustrated in Figure 4 (lower panel), the percentage of live S. pyogenes was 93.2% in the untreated control bacterial strain. In contrast, the percentage of live *P. aeruginosa* was 91.7% following treatment with ZnO NPs at 125 µg/mL. These percentages dropped to 7.92 and 10.2%, respectively.

3.4 Antiviral activity of ZnO NPs

First of all, the cytotoxicity of ZnO NPs against MDCK cells was measured by MTT assay, as indicated in Figure 5a. At concentrations up to $100\,\mu\text{g/mL}$, cell viability was unaltered. The effects of pre-treatments with ZnO NPs were measured by investigating the neuraminidase activity, as shown in Figure 5b. The results showed that ZnO NPs reduced neuraminidase activity in a concentration-dependent manner. In this study, flow cytometry results indicated that ZnO NPs are capable of reducing apoptosis induced by the H1N1 influenza A virus in MDCK cells, as shown in Figure 5c. These results present evidence for the

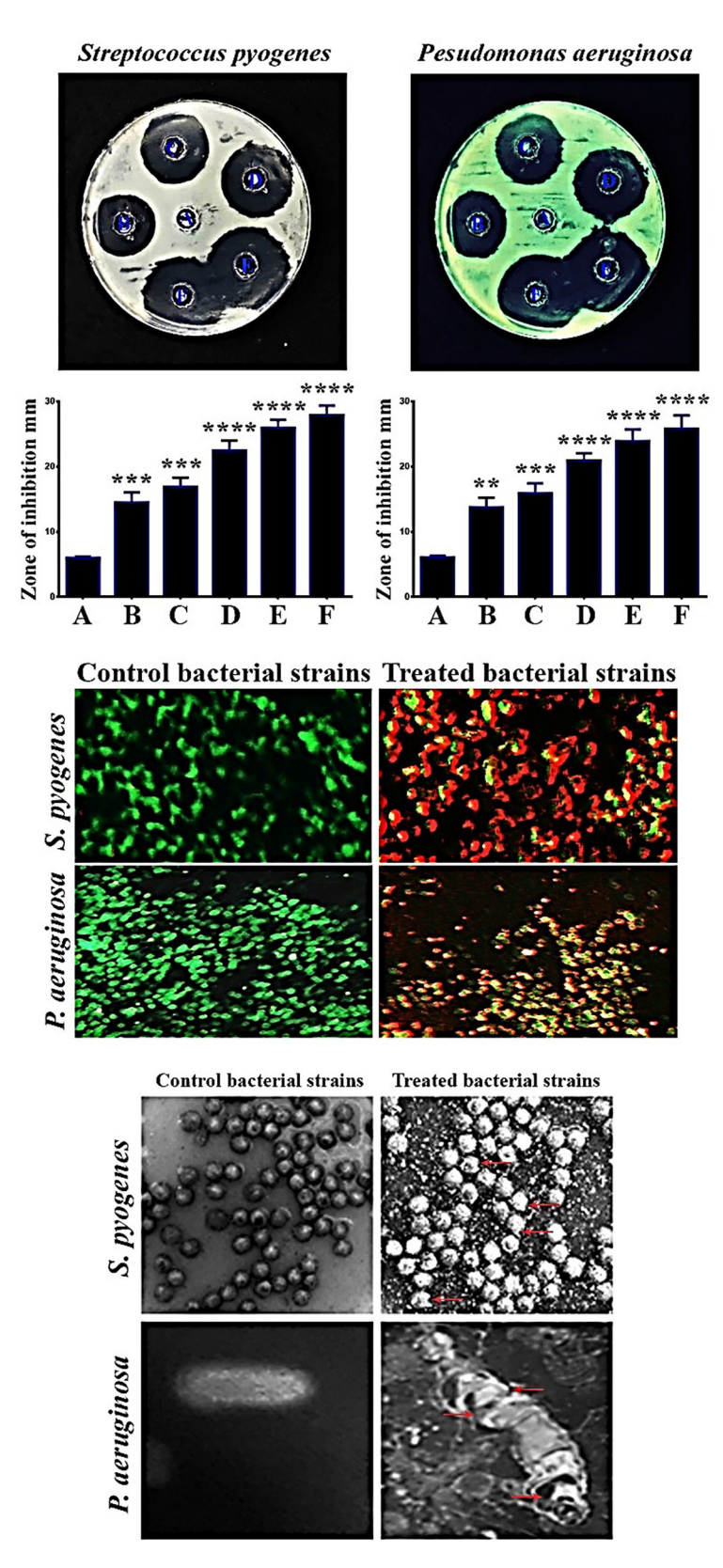


Figure 3: ZnO NPs inhibit growth of S. pyogenes and P. aeruginosa. (A) Control untreated bacterial strain, (B)–(F) bacterial strain treated with ZnO NPs at 31.25, 62.5, 125, 250, and 500 µg/mL, respectively (Upper panel). Data are shown as the mean value ± standard deviation of three different experiments. $p \le 0.01$ **, $p \le 0.001$ ***, $p \le 0.0001$ ***. Middle panel represented live and dead bacterial strain using AO/EtBr staining. Lower panel represented how ZnO NPs alter the morphology of bacteria. Red arrows indicate damaged bacterial strains.

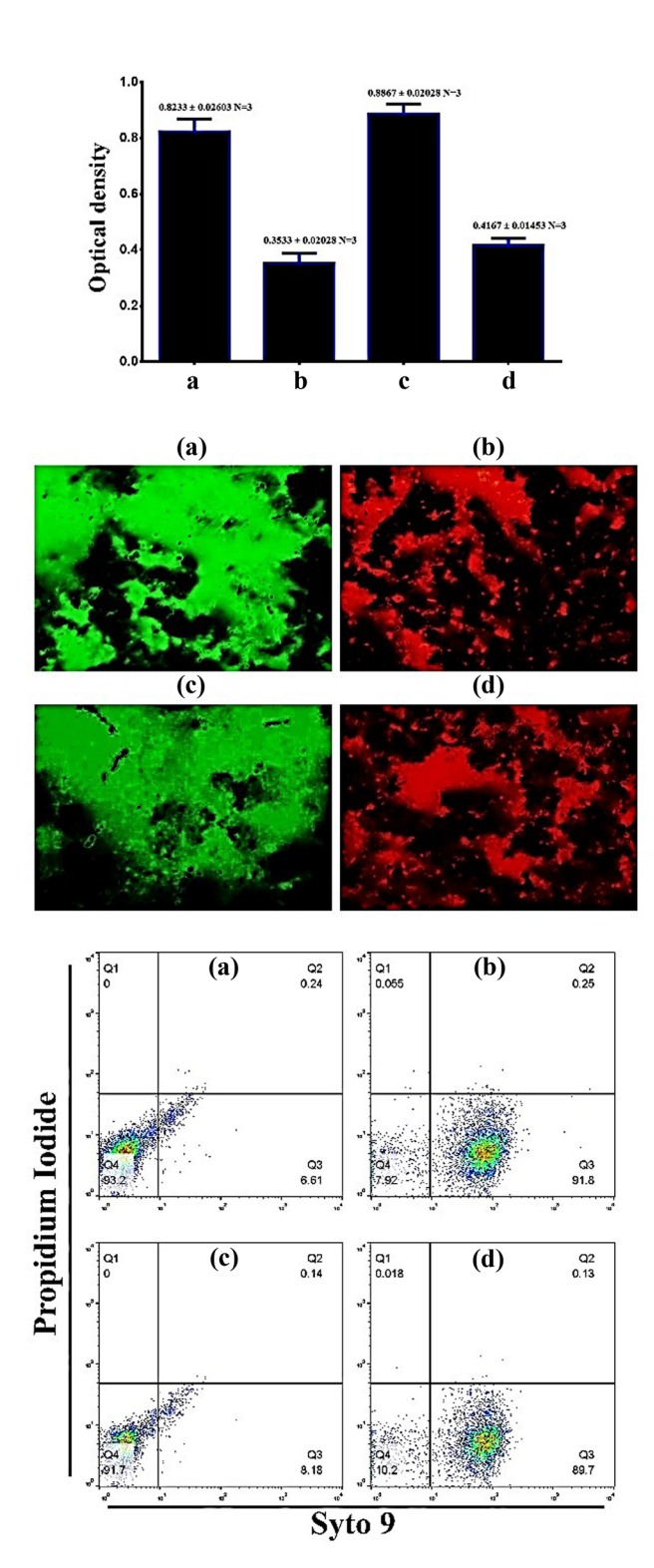


Figure 4: ZnO NPs reduce biofilm formation of *S. pyogenes* and *P. aeruginosa*. (a) Control untreated *S. pyogenes*, (b) *S. pyogenes* treated with ZnO NPs at 125 μ g/mL, (c) control untreated *P. aeruginosa*, and (d) *P. aeruginosa* treated with ZnO NPs at 125 μ g/mL. Data are indicated as the mean value \pm standard deviation of three different experiments.

antiviral activity of silver ZnO NPs. The ROS generation was measured using a flow cytometry assay, as indicated in Figure 5d; the ROS generation by the H1N1 influenza virus was significantly increased, and after being treated with ZnO NPs, the ROS generation was inhibited. These results show that ZnO NPs could downregulate the level of ROS in the antiviral activity.

3.5 Antioxidant activity of ZnO NPs

The antioxidant activity of ZnO NPs is demonstrated in Figure 5. The higher concentrations of ZnO NPs resulted in an enhancement of both DPPH and ABTS radical scavenging capabilities. At concentrations below 100 $\mu g/mL$, respectively, the ZnO NPs scavenged more than 40% of the ABTS and DPPH free radicals, as indicated in Figure 6. The ZnO NPs have the ability to function as both an electron donor and an acceptor.

3.6 ZnO NPs inhibits Type 2 diabetes

Using the amylase enzymatic inhibition assay, the antidiabetic activity of the ZnO NPs was evaluated. As shown in Figure 7 (upper left panel), these ZnO NPs showed excellent inhibition when tested at various concentrations ranging from 0 to 150 µg/mL. ZnO NPs proved almost 50% antidiabetic effectiveness at a 50 µg/mL concentration. In the current study, we assessed the potential therapeutic benefits of zinc oxide on streptozotocin-induced diabetic mice. According to our findings, the blood glucose levels of the diabetic groups treated with ZnO NPs, significantly decreased by almost 150 mg/dL, compared to the diabetic mice group by almost 350 mg/dL as indicated in Figure 7 (upper right panel). The results showed the ability of ZnO NPs to induce GK activity as in Figure 7 (lower left panel). For histopathological changes of spleen sections, the control group showed a normal pancreas section. Meanwhile, the diabetic group indicated damaged and destructed islets of Langerhans, with damage in pancreas cells. In the diabetic + ZnO NPtreated group, the pancreas was less destructed as shown in Figure 7 (lower right panel). Therefore, ZnO NPs have excellent antidiabetic potential and may effectively treat diabetic wounds.

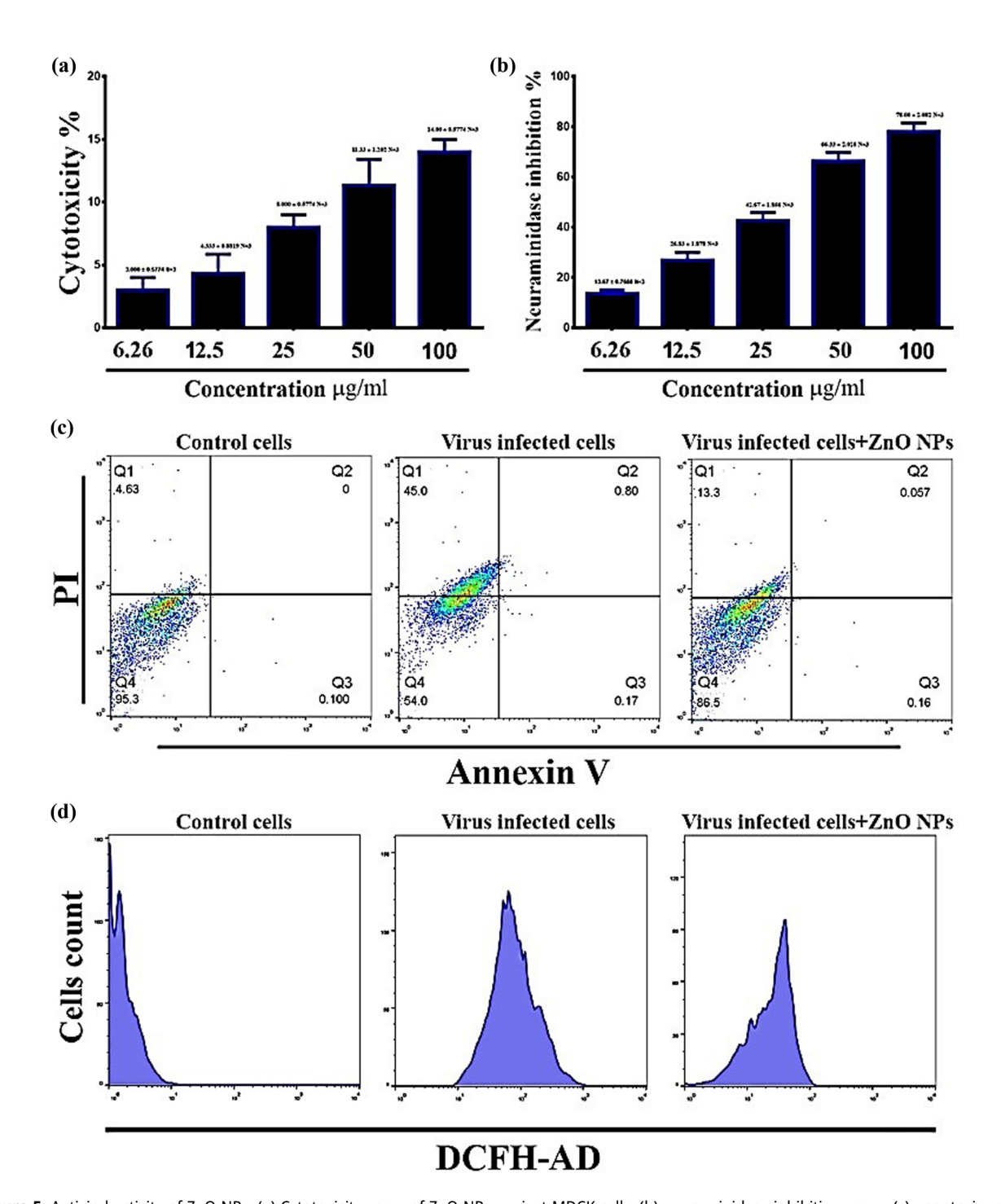


Figure 5: Antiviral activity of ZnO NPs: (a) Cytotoxicity assay of ZnO NPs against MDCK cells, (b) neuraminidase inhibition assay, (c) apoptosis assay using Annexin V, and (d) ROS generation assay using DCFH-AD. Data are indicated as the mean value ± standard deviation of three different experiments.

3.7 ZnO NPs induce phagocytosis

BMDMs were isolated, and the ability of these phagocytic cells to phagocytose *Candida albicans* was tested. The results revealed that the ratio of BMDM cells that were treated with ZnO NPs to phagocyte *Candida albicans* was

significantly higher than that in the BMDM cells untreated with ZnO NPs (p < 0.001), as indicated in Figure 8 (left panel). To study the effect of ZnO NPs in phagosome maturation via evaluating the Lysotracker red, which labels late endosomes and lysosomes specifically, additional loading of BMDMs made it possible to examine the

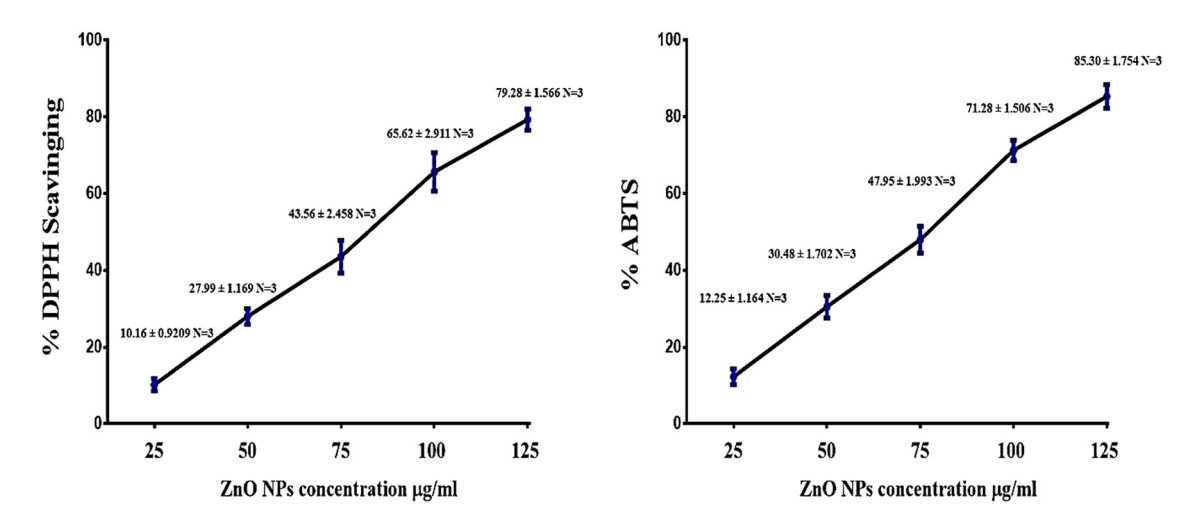


Figure 6: Antioxidant activities of ZnO NPs. Data are indicated as the mean value ± standard deviation of three different experiments.

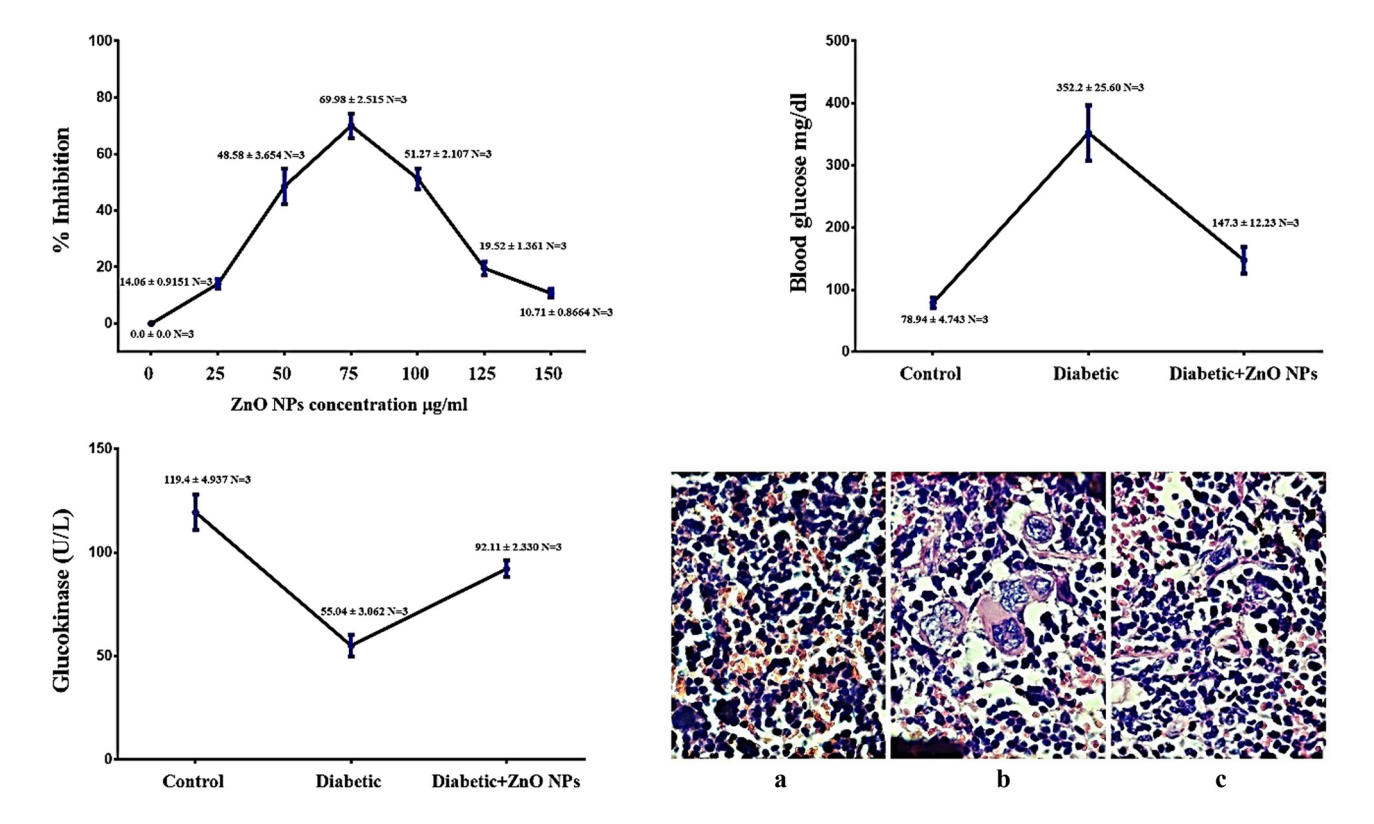


Figure 7: Anti-diabetic activity of ZnO NPs. Upper left panel shows the ability of ZnO NPs to inhibit the α-amylase activity. Upper right panel shows the ability of ZnO NPs to reduce glucose level. Lower left panel shows the ability of ZnO NPs in induction of GK activity. Data are indicated as the mean value ± standard deviation of three different experiments. While lower right panel showed histopathological changes in spleen sections. (a) Control. (b) Diabetic group. (c) ZnO NP-treated diabetic group.

maturation activities of the *S. aureus*-FITC ingesting phagosomes. Co-localization with Lysotracker Red over time capabilities. The findings showed that this co-localization occurred in BMDMs that had been pretreated with ZnO NPs for 2 h. Simultaneously, in control BMDMs, the majority of *S. aureus*-FITC entities had less co-localization with the Lysotracker, as indicated in Figure 8 (right panel). The ability of BMDMs to phagocytose bacteria was investigated *via* the observation of the uptake of tagged *E. coli*, which was unable to emit fluorescence until their transfer into the

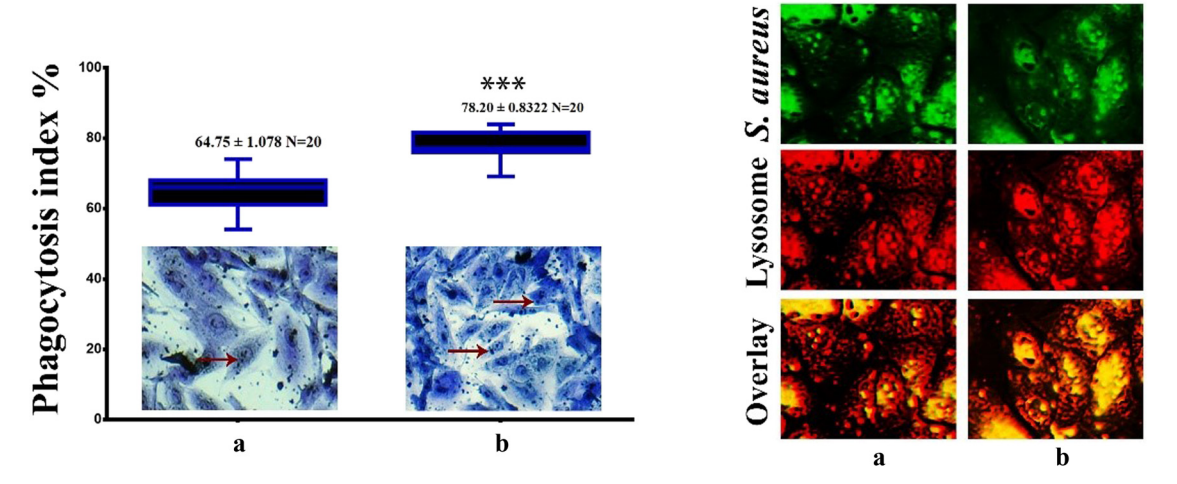


Figure 8: ZnO NPs enhanced phagocytosis ability against *C. albicans* and *S. aureus*. (a) Control BMDMs, (b) BMDMs in the presence of ZnO NPs. Red arrows indicated *C. albicans* inside phagocytic cells. Data are indicated as the mean value \pm standard deviation of three different experiments. $p \le 0.001$ ***.

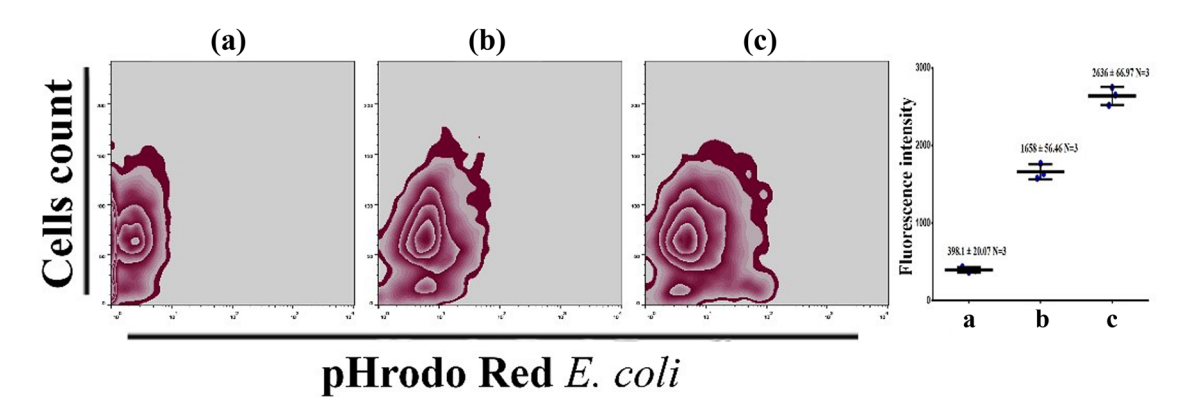


Figure 9: ZnO NPs enhanced the BMDMs to engulf pHrodo *E. coli* particles. (a) Control untreated BMDMs, (b) BMDMs treated pHrodo *E. coli* particles. (c) BMDMs treated pHrodo *E. coli* particles in the presence of ZnO NPs. Data are indicated as the mean value ± standard deviation of three different experiments.

lysosome (low pH), as indicated in Figure 9. Phagocytosis of the pHrodo *E. coli* bioparticles was compared following BMDM pre-treatment with ZnO NPs at a concentration of 25 µg/mL. The control untreated BMDM cells showed lower phagocytotic activity as compared to pretreated with ZnO NP BMDM cells. The results of the current study prove the ability of ZnO NPs to enhance the treated BMDM cells to phagocytose and kill the bacteria. This experiment aimed to test how pre-treatment with ZnO NPs could stimulate the ability of BMDMs to phagocytose pHrodo *E. coli* bioparticles. We also aimed to test the mechanisms that could be involved in this process. Taken together, the results demonstrated that pre-treatment with ZnO NPs increases the ability to produce phagocytosis. This suggests that the ability of BMDMs to kill microorganisms could be enhanced.

3.8 ZnO NPs induce autophagy and inhibit inflammasome (NLRP3) activity

We hypothesized that once BMDM cells were pretreated with ZnO NPs following LPS and ATP, they would increase autophagy. Using immunofluorescence tests, we investigated the expression of LC3, a significant autophagy-related protein, to ascertain whether BMDMs treated with ZnO NPs trigger autophagy. Our findings showed that after treating LPS + ATP, BMDMs showed autophagy LC3 marker. In cells that had been pre-treated with ZnO NPs, the absolute amount of LC3 increased. The localization of endogenous LC3 to autophagy vacuoles was studied using immunofluorescence, as demonstrated in Figure 10 (upper panel). In the current study, we hypothesized that ZnO NPs' impact on

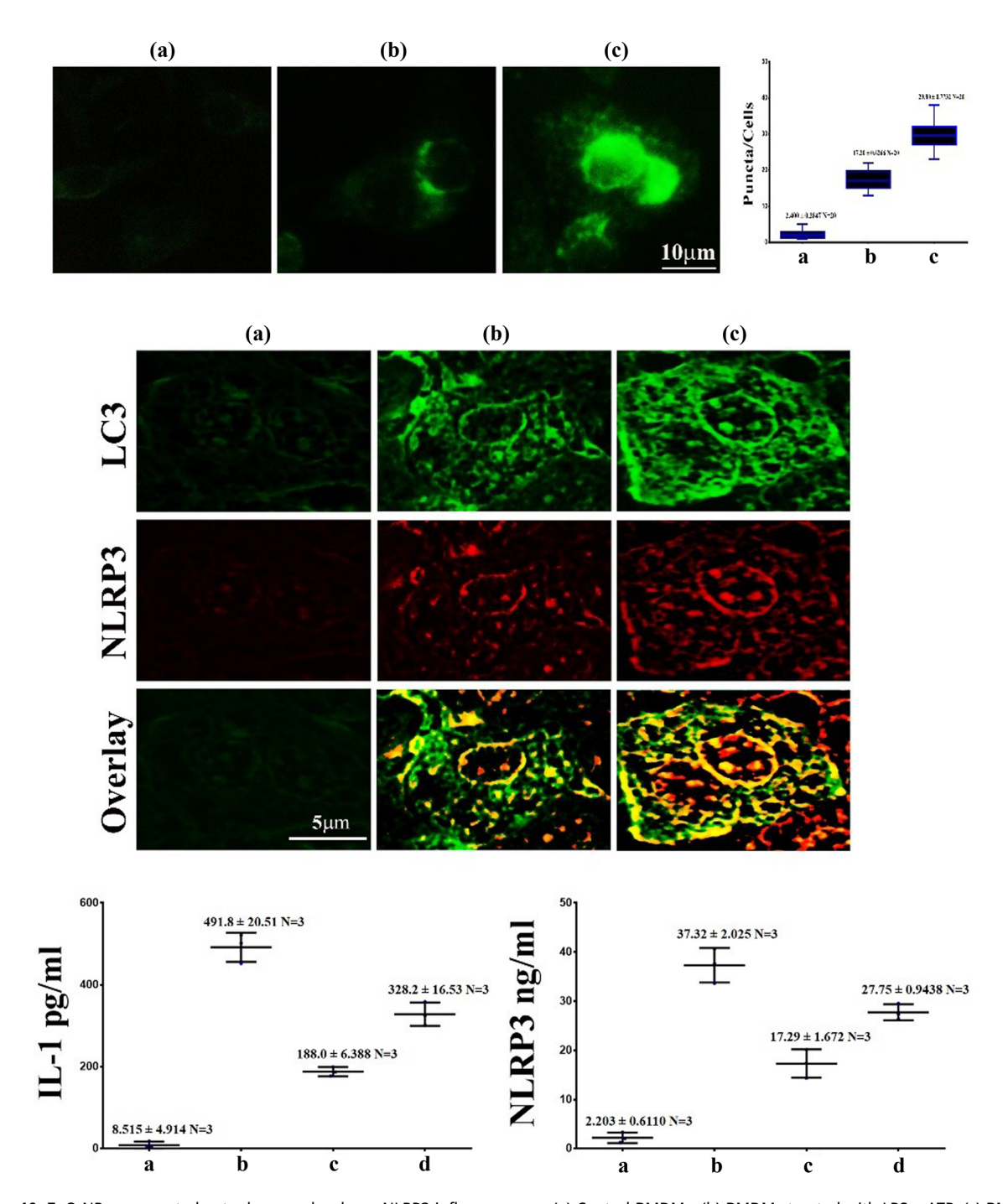


Figure 10: ZnO NPs augmented autophagy and reduces NLRP3 inflammasome. (a) Control BMDMs, (b) BMDMs treated with LPS + ATP, (c) BMDMs treated with LPS + ATP in the presence of ZnO NPs, and (d) BMDMs treated with LPS + ATP in the presence of ZnO NPs + 3-MA. Data are indicated as the mean value ± standard deviation of three different experiments.

autophagy could modify the activation of NLRP3 inflamma-some. The results showed that BMDMs pretreated with ZnO NPs following treatment with 500 μ g/mL LPS + 5 mM ATP exhibited significantly lower IL-1 and NLRP3 levels, as indicated in Figure 11. Next we tested how ZnO NPs improved NLRP3 degradation by autophagy. After BMDM cells were treated with LPS + ATP, we assessed the amount of NLRP3

inflammasome, either with or without the addition of ZnO NPs. The NLRP3 inflammasome was found to be reduced in BMDM cells that were exposed to both ZnO NPs and LPS + ATP combination therapy, as shown in Figure 10 (middle panel). The results demonstrated the occurrence of significant co-localization between LC3 and NLRP3 in the presence of ZnO NPs. These results demonstrate that the ZnO NPs

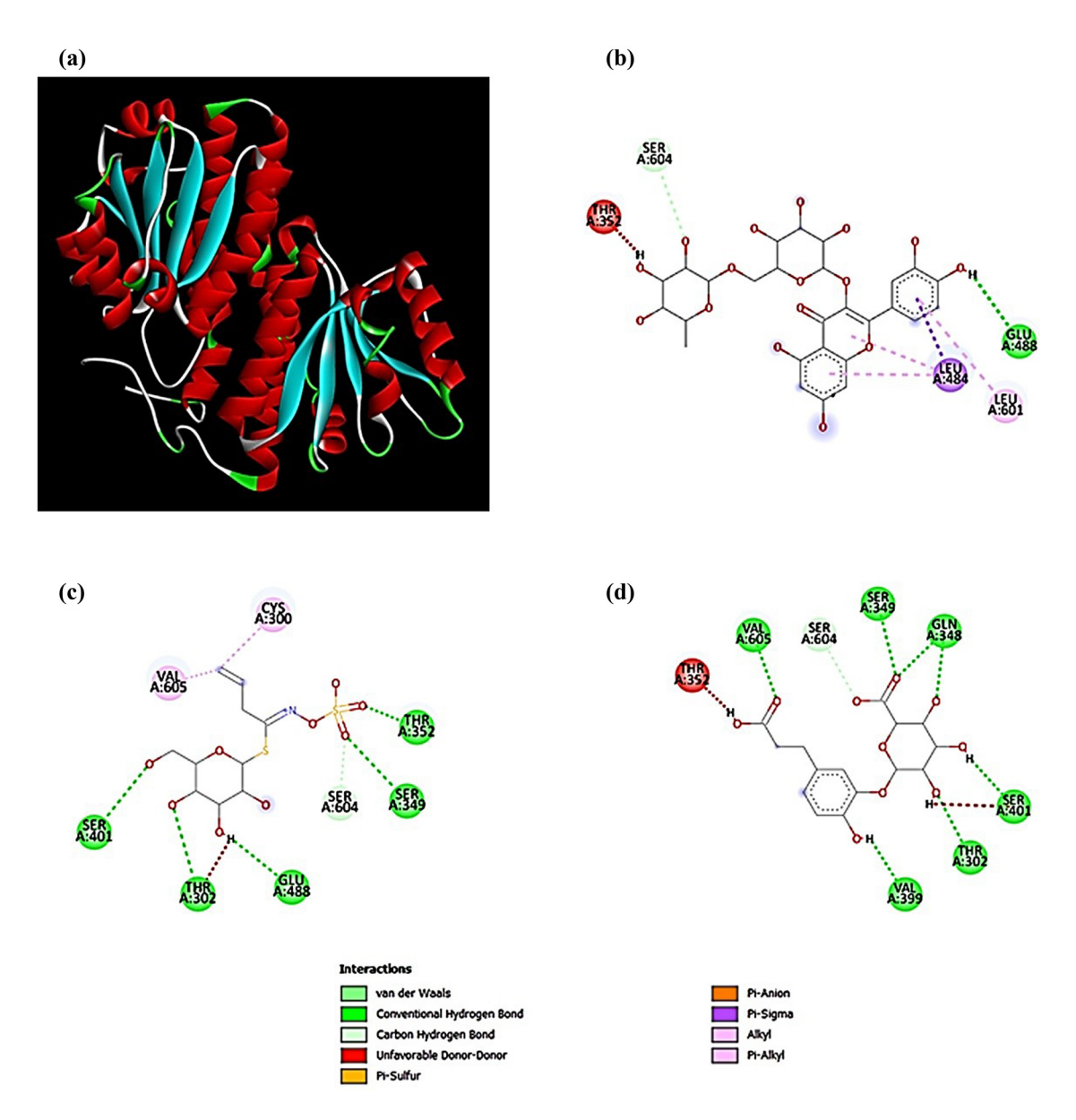


Figure 11: Binding the three bioactive compounds of red radish inside the GlcN-6-P synthase (PDB:1MOQ) active site. (a) Structure of GlcN-6-P synthase, (b) rutin inside the binding site, (c) sinigrin inside the binding site, and (d) dihydrocaffeic acid 3-0-glucuronide.

caused the increase in autophagy and the NLRP3 inflammasome and IL-1 degradation. This study thus shows that in LPS + ATP-treated BMDM cells, autophagy plays a crucial role in regulating the release of NLRP3 and IL-1. In the current work, we also investigated the effects of autophagy suppression on inflammasome activation in cells that were treated in combination with ZnO NPs and LPS + ATP. The use of 3-methyladenine (3-MA) at a concentration of 10 mM to inhibit autophagy led to increased activation of inflammasomes in cells treated with both ZnO NPs and LPS + ATP together. The results indicated that there was a significant increase in NLRP3 and IL-1 levels, as indicated in Figure 10 (lower panel). These results show that after treatment with

LPS + ATP in the presence of ZnO NPs, a lack of autophagy increases the activation of inflammasomes.

3.9 Docking study results

3.9.1 Docking against GlcN-6-P synthase

The active components extracted from the red radish, rutin, sinigrin, and dihydrocaffeic acid 3-O-glucuronide, were in silico docked inside the active site of GlcN-6-P synthase (PDB:1MOQ) after the removal of the crystal structure of glucosamine-6-phosphate to explain the interaction mode and the binding affinity toward the enzyme. The docking outcomes indicate that rutin exhibited the best binding energy equal to 8.4 kcal/mol. The other active ingredients (sinigrin and dihydrocaffeic acid 3-O-glucuronide) have binding energies of -7.7 and 8.1 kcal/mol, respectively. The interaction types for the three active ingredients within the binding pocket of the enzyme are shown in Figure 11. As illustrated in Figure 11, there are several interactions between the Rutin and the active site of the enzyme. Rutin binds the GLU:488A residue with one hydrogen bond and one non-classical hydrogen bond with SER:A:604. There are three alkyl pi interactions between rutin and the LEU:A:484 and LEU:A:601 residues. The last favored interaction was between the phenyl moiety of the rutin and the LEU:A:601 residue as pi sigma interaction. The red dashed line represents the unfavorable interactions.

3.9.2 Docking against estrogen receptor

The present study includes docking of the three bioactive components in the red radish extracts inside the binding pocket of ER alpha. The molecular docking was done to analyze the selectivity of three ligands, rutin, sinigrin, and dihydrocaffeic acid 3-O-glucuronide, toward the ER alpha. The binding affinities for the best binding conformer were -8.6, -7.0, and -6.9 kcal/mol for the rutin, sinigrin, and dihydrocaffeic acid 3-O-glucuronide, respectively. The rutin exhibited the best binding affinity compared with the other compounds. The three compounds bind the active site with several bonds, including H-bonds and hydrophobic interactions. The rutin binds the active site with four hydrogen bonds with the CYS350, MET522, and MET528, while there are several hydrophobic interactions, including the following residue: ALA350, LEU354, TRP383, LEU525, and LEU536. Figure 12 shows the binding of the three red radish components within the binding site of ER alpha.

3.9.3 Docking against tubulin

Three active components of red radish, rutin, sinigrin, and dihydrocaffeic acid 3-O-glucuronide were modeled as colchicine analogs based on the knowledge of the structure—activity relationship between colchicine and tubulin. Colchicine analogs have the ability to attach to tubulin and prevent its polymerization, which can result in disrupted mitosis, a sudden disruption of mitotic spindle assembly, and interference with the cytoskeleton's usual

function. Therefore, the current study also included the molecular docking studies of rutin, sinigrin, and dihydrocaffeic acid 3-O-glucuronide toward tubulin colchicine binding site (402B) to study the action mechanism of this new skeleton as anticancer agents. The binding affinities for the best binding conformer were -9.8, -7.7, and -9.1 kcal/mol for the rutin, sinigrin, and dihydrocaffeic acid 3-O-glucuronide, respectively. The rutin exhibited the best binding affinity compared with the other compounds. The three compounds bind the active site with several bonds, including H-bonds and hydrophobic interactions. Rutin binds the active site with three hydrogen bonds, including the flowing residues: ASP:A:69, ASN:A206, and LYS:B254. There are two hydrophobic interactions with ALA:B250 and LYS:B:254. Furthermore, rutin binds the GLN:A:11 and GLY:A:10 with a pi donor hydrogen bond and one carbon-hydrogen bond, respectively. Figure 13 shows all the interactions between the colchicine binding site of tubulin and the two active components of red radish.

4 Discussion

Because ZnO NPs are inexpensive, biocompatible, and have minimal toxicity, they are frequently utilized in a variety of biological applications. It has been demonstrated that ZnO NPs have antibacterial and anticancer properties. Notably, synthesizing ZnO NPs from plant extracts is a good option against bacterial growth and proliferation of cancer cells. ZnO NPs of *R. sativus* could be a novel source of chemopreventive agents [50].

4.1 Anticancer effects

The present study revealed that ZnO NPs led to dose-dependent cytotoxicity against cancer cell lines. The ZnO NPs had a lower IC $_{50}$ concentration for A549 cancer cells than MCF-10 cells, which suggests that the NPs are selectively toxic against cancer cell line rather than normal cell line. AO/EtBr staining assays were done to measure the viability of cancer and normal cell lines. For the AO/EtBr assay, A549 cells were exposed to ZnO NPs at a concentration of 22.78 μ g/mL. The results exhibited that the untreated control A549 cells were stained with AO (Green), indicating that they were living cells. As shown in Figure 2 (middle panel), the ZnO NP-treated A549 cells were stained with EtBr, a yellow-orange dye that denotes dead cells. No changes were observed in the normal cell line (MCF-10)

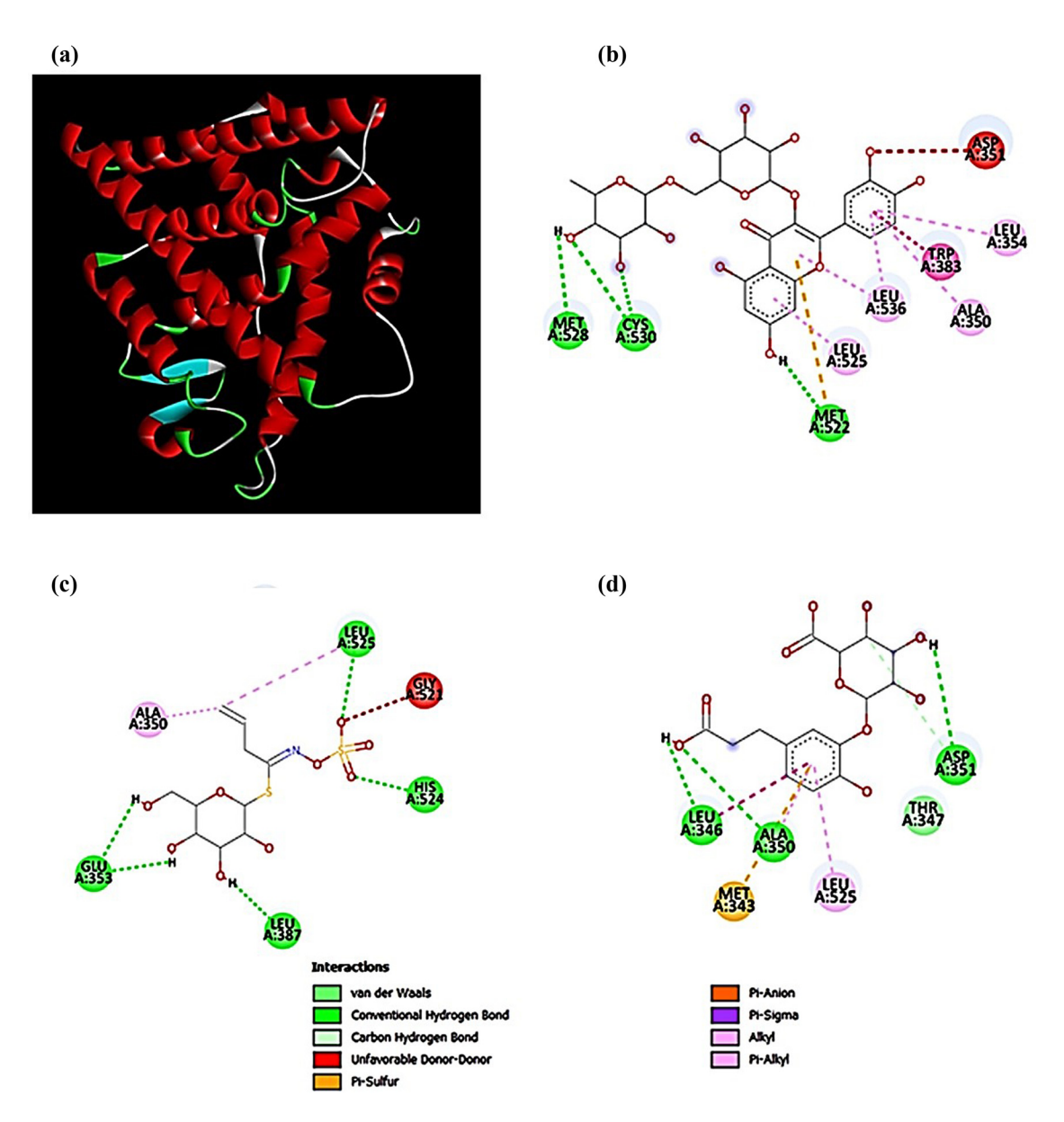


Figure 12: Binding the three bioactive compounds of red radish inside the estrogen receptor (PDB:3ERT) active site. (a) Structure of estrogen receptor, (b) rutin inside the binding site, (c) sinigrin inside the binding site, and (d) dihydrocaffeic acid 3-*O*-glucuronide.

after being treated with ZnO NPs. To study the ability of ZnO NPs in apoptosis gene expression, we investigated p53, BAX, and BCL-2 levels. The outcomes showed the ability of prepared ZnO NPs to upregulate and downregulate apoptosis proteins, as shown in the lower panel of Figure 2. The cytotoxicity of ZnO NPs has been demonstrated in previous published study on diverse cancer cell lines through increased oxidative stress, intracellular Ca²⁺ level, and decreased membrane permeability transition (MPT) [51]. This cytotoxicity was caused by the ability of NPs to increase intracellular Ca²⁺ levels. ZnO NPs excite an increase in interleukin (IL-8) production in both the BEAS-2B bronchial epithelial cells and the A549 alveolar adenocarcinoma cells

[52–54]. In addition, the MPT, the loss of membrane integrity, and the activation of the p53 pathway are all reduced in RAW264.7 cells when ZnO NPs are present [55]. Furthermore, ZnO NPs can produce a wide array of proinflammatory indicators in the mononuclear cells of the peripheral blood [56]. These mediators include interferon-c, tumor necrosis factor- α (TNF- α), and IL-12. Furthermore, murine RAW264.7 macrophages and murine dendritic cells (DCs) produced from bone marrow have increased IL-1 and the chemokine CXCL9 expression in response to ZnO NPs [57]. In addition to cytotoxicity, ZnO NPs also cause a range of genotoxicity in different cell types. For example, they cause DNA damage in human epidermal cells A431, micronuclei

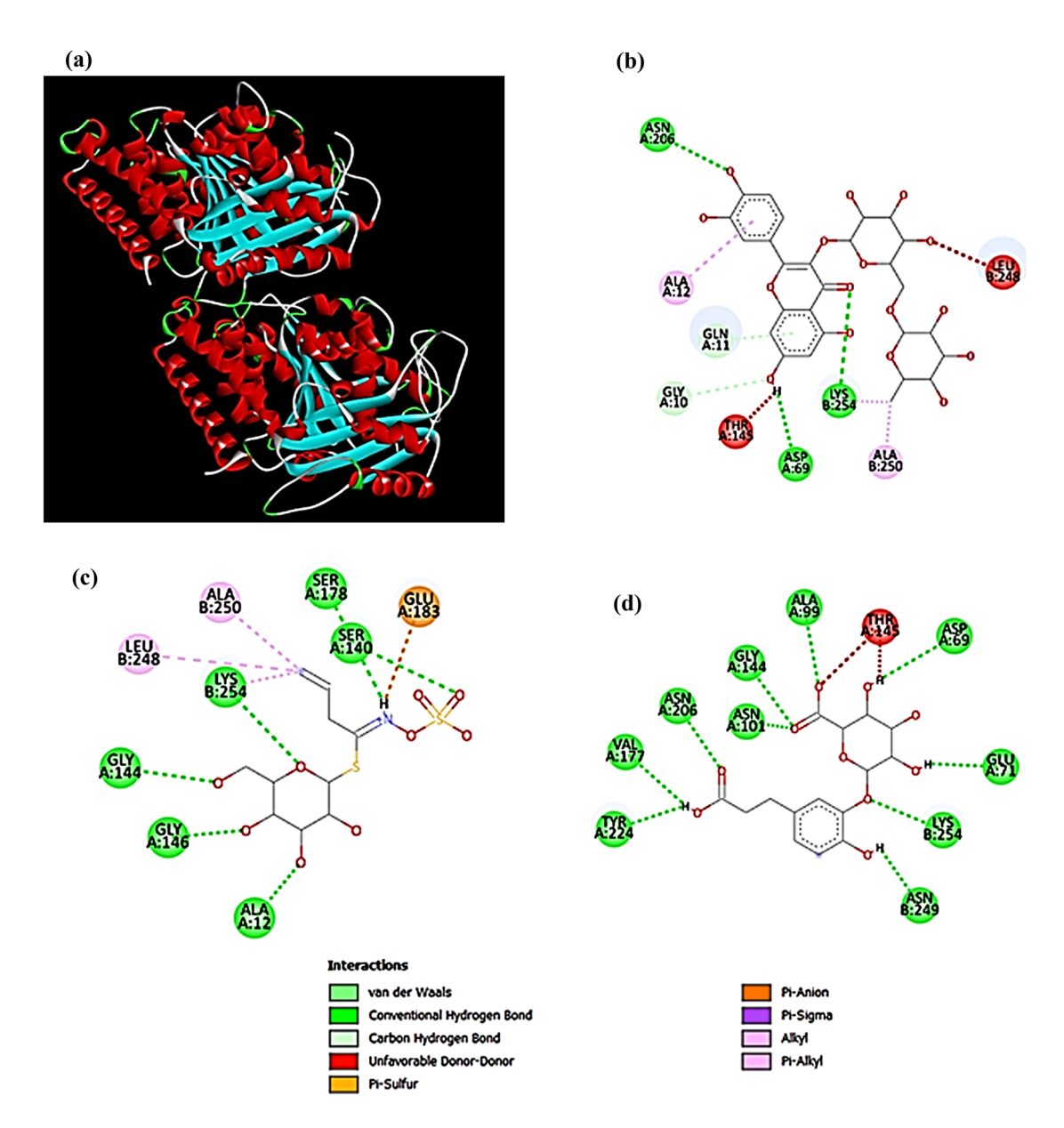


Figure 13: Binding the three bioactive compounds of red radish inside the tubulin receptor (PDB:402B) active site. (a) Structure of tubulin receptor, (b) rutin inside the binding site, (c) sinigrin inside the binding site, and (d) dihydrocaffeic acid 3-*0*-glucuronide.

formation, phosphorylation of H2AX, and DNA damage in human SHSY5Y neuronal cells [58]. Likewise, ZnO NPs cause damage to A431 cells' DNA [59]. Several investigations have demonstrated the participation of many signaling pathways, including p38 mitogen-activated protein kinase, extracellular signal-related kinase, and c-Jun N-terminal kinase, in the oxidative stress-specific apoptosis produced by ZnO NPs [60]. This conclusion was reached because ZnO NPs induced apoptosis [61]. These findings indicated that ZnO NPs could activate proapoptotic proteins, which led to the induction of the mitochondrial apoptotic pathway [62]. ZnO NPs display higher anti-tumor and anti-proliferative activity against

cancer cells through the induction of ROS, which causes oxidative stress and eventually leads to cell death [63]. This property distinguishes ZnO NPs from other types of metal NPs. Oxygen metabolites, or ROS, are highly potent oxidative adulterants that can be applied to biological macromolecules like proteins, lipids, and polynucleotides. When there is an imbalance between ROS production and the cell's antioxidant system, cellular redox homeostasis cannot be maintained [64,65]. This is because indiscriminate oxidation can occur when there is an imbalance, resulting in "oxidative stress." ROS production must be kept in check to maintain this balance [66]. Several

studies demonstrated that an abnormally high level of oxidative stress is hazardous to the cell and results in severe cytotoxicity [67,68]. In a cell, ROS is produced in the mitochondria. ROS seriously harms macromolecules in cells, especially DNA. The loss of mitochondrial membrane potential (MPT), which exposes cytochrome c to the intermembrane gap, triggers the activation of caspases [69]. Cytochrome c leaks as a result of exposure, and this triggers the activation of caspases [70]. As a result, ROS plays a significant and vital role in the processes that lead to cell death, apoptosis, and autophagy [71]. Cell death may ultimately ensue from an overabundance of autophagy and cellular self-consumption resulting from cellular damage. Notably, ROS has bidirectional effects on cancer cells, promoting apoptosis or enhancing tumorigenesis [71]. During cancer progression and metastasis, cancer cells adapt to the effect of high oxidative stress by increasing NADPH expression and reducing folate metabolism. Arfin et al. [70] demonstrated that high oxidative stress promotes the expression of pro-tumorigenic signaling, leading to DNA injury and genetic instability. Higher oxidative stress reduces rather than increase the proliferation of cancer cells. Therefore, ZnO NP-induced ROS might be the potential mechanism for cytotoxicity against cancer cells.

4.2 Antibacterial effects

In the current work, the effect of ZnO NPs as antibacterial agent has been evaluated against S. pyogenes and P. aeruginosa. Taken together, ZnO NPs inhibit bacterial growth in a concentration-dependent manner, as shown in Figure 3, upper panel. Bacterial stains could be killed and destroyed by ZnO NPs via many factors like size and the morphology of NPs, and also based on the kind of bacterial strains. Fluorescence microscopy was used to distinguish between live and dead bacterial strains using AO/EtBr double staining assay. AO is responsible for staining live cells. While EtBr was responsible for the stain of dead bacterial strains. For both bacterial strains, as in Figure 2 lower panel, all untreated bacterial stains appeared green, and following treatment with ZnO NPs, the bacterial strain appeared orange-red. SEM was utilized to investigate how ZnO NPs affected the development and structure of bacterial strains. Figure 3 lower panels show differences between the ZnO NP-treated bacteria and control samples. The results show that a control untreated bacterial strain displayed cluster-form colonies. SEM images show that S. pyogenes and P. aeruginosa would be destroyed by ZnO NP treatment, as shown in Figure 3, lower panel. The synthesized NPs under study exhibit notable antimicrobial activity. Damaged colonies have an impact on the bacterial strains. The bacterial strains with damaged membranes were penetrated and stained with PI stain fluorescence dye, while the membranes in good condition were stained by Syto 9 green fluorescence dye. Untreated control bacterial strains assembled and formed a developed biofilm layer; the ZnO NPs at a concentration of 125 µg/mL had a less dense biofilm coating and were less aggregated. The results of the current study highlight the impacts of ZnO NPs, as well as their ability to prepare ZnO NPs to suppress biofilm formation. Using a flow cytometry technique, the biofilm metabolic activity of bacterial strains was examined as indicated in Figure 4. Findings of the present study demonstrated that ZnO NPs were effective against S. pyogenes and P. aeruginosa in a concentration-dependent manner but were powerfully affected by the size and the topology of ZnO NPs. It has been shown that ZnO NPs were effective against Escherichia coli in a concentration-dependent manner through ROS-induced membrane lipid peroxidation [72]. Besides, da Silva et al. [73] reported that the size and surface modification affected the antibacterial activity of ZnO NPs. Decreasing the size of ZnO NPs increases their antibacterial activity against E. coli and S. aureus. Therefore, smaller ZnO NPs <5 nm have bactericidal effects, while larger ZnO NPs have bacteriostatic effects [74]. Therefore, smaller ZnO NPs have better antimicrobial properties than the larger ones. Besides, the synthesis of spherical ZnO NPs by the precipitated method had more potent antibacterial activity than commercial ZnO NPs. Remarkably, chronic exposure of E. coli to a low concentration of ZnO NPs induces a robust antibacterial activity compared to a single higher concentration of ZnO NPs [74]. In vitro study demonstrated that exposure of E. coli to 0.06 mg/mL of ZnO NPs led to two-fold inhibition of bacterial growth compared to the single higher concentration of ZnO NPs 0.30 mg/mL [75]. The antibacterial activity of ZnO NPs is related to the generation of ROS and lipid peroxidation of bacterial cell walls. Jiang et al. [76] observed that ZnO NPs exert bactericidal activity against Gram-positive and Gram-negative by inducing membrane dysregulation via the release of zinc and hydrogen peroxide. Numerous investigations used SEM and FESEM to analyze the morphological changes in bacteria treated with NPs, such as ZnO NPs. ZnO NPs' antimicrobial activity relies on ZnO-NPs making direct contact with the cell walls, which destroys the integrity of the bacterial cell [77]. SEM analysis was used to examine the morphological changes in the bacterial strains before and after they were treated with nanorods. α -Mn₂O₃ NPs were investigated as antimicrobial agent.

significant morphological changes were showed in all examined bacterial strains. Naskar et al. produced Ni + 2-doped ZnO NPs for their study. A. baumannii ATCC 19606, S. aureus ATCC 25923, S. epidermidis ATCC 12228, and E. coli ATCC 25922 were used to investigate the produced NPs' antibacterial activity [78]. According to the results, the growth of microbiological strains was strongly inhibited by ZnO NPs. These decreases in the development of biofilms could be connected to the process that produces ROS. These ROS have the power to peroxide and oxidize lipids and proteins, weakening the membrane of Gram-negative cells, altering fluid permeability and ion transport, and interrupting metabolic activities. Moreover, direct or electrostatic interaction between the bacteria and the NPs may damage the outer membrane of Gram +ve and Gram -ve bacteria. In sum, these findings, together with the present study's findings, indicated that ZnO NPs have potent antibacterial activity.

4.3 Antiviral activity of ZnO NPs

These results of the current study indicate the antiviral activity of ZnO NPs. The ROS generation was measured using a flow cytometry assay, as shown in Figure 5; the ROS generation by the H1N1 influenza virus was significantly increased, and after exposure to ZnO NPs, the ROS generation was inhibited. The present study's findings illustrated that ZnO NPs reduced neuraminidase activity in a concentration-dependent manner, reducing apoptosis induced by the H1N1 influenza A virus in MDCK cells. Notoriously, the present study revealed that ZnO NPs downregulate the level of ROS in their antiviral activity. Many preclinical studies have shown that ZnO NPs have potent antiviral activity [79-81]. ZnO NPs from the alcoholic extract of Plumbago indica L. showed antiviral activity against herpes simplex virus 1 (HSV-1) in a concentration-dependent manner [82]. Likewise, an *in silico* study demonstrated that hesperidin ZnO NPs have a significant antiviral effect against hepatitis A virus (HAV) [83]. Cotton fabrics ZnO NPs have antiviral activity against HSV-1, adenovirus, and coxsackie B virus about the antiviral acyclovir. Supporting the present study, Ghaffari and his colleagues demonstrated that PEGylated ZnO NPs are effective and novel antiviral in managing H1N1 influenza viral infection [84]. The viricidal mechanism of ZnO NPs is mediated by the release of zinc and various types of ROS. In addition, ZnO NPs modulate virus transcription and alter membrane polarity prompted by the negative charge of ZnO and positive charge of virus capsid protein. Furthermore, ZnO NPs inhibit viral RNA transcription of the chikungunya virus [85]. Notoriously, ZnO NPs can interfere with the replication and entry of SARS-CoV-2.

4.4 Antioxidant effects

Antioxidant functionalization does not alter the intrinsic antioxidant properties of many NMs; instead, their qualities depend on their surface features. The most widely employed antioxidant NMs are inorganic metal NPs, especially those made using the green synthesis methods [86]. Eucalyptus globulus produces antioxidant ZnO NPs as capping and reducing agents for photocatalytic uses. The capping of natural compounds on the ZnO surface and smaller particle size can increase the antioxidant activity of these materials compared to those generated by standard chemical methods. Aldehyde with cuminic acid and Eucalyptus globulus's sitosterol significantly affected ZnO NPs antioxidant activity [87].

4.5 Antidiabetic activity of ZnO NPs

ZnO NPs as antidiabetic agent was investigated. As shown in Figure 7, these ZnO NPs showed excellent inhibition when tested at different doses from 0 to 150 µg/mL. ZnO NPs proved to be almost 50% antidiabetic effective at a 50 μg/mL concentration. The blood glucose levels of the diabetic groups treated with ZnO NPs, significantly decreased by almost 150 mg/dL, compared to the diabetic mice group by almost 350 mg/dL as indicated in Figure 7 (upper right panel). The results showed the ability of ZnO NPs to promote GK activity as shown in Figure 7 (lower left panel). For histopathological changes of spleen sections, the control group showed a normal pancreas section. Meanwhile, the diabetic group indicated damaged Langerhans islets, with damage in pancreas cells. In the diabetic and ZnO NPtreated group, the pancreas was less destructed as shown in Figure 7 (lower right panel). Therefore, ZnO NPs have excellent antidiabetic potential and may effectively treat diabetic wounds. In the current work, we assessed the potential therapeutic benefit of ZnO NPs on streptozotocininduced diabetic mice. The blood glucose levels in the diabetic groups treated with ZnO NPs (150 mg/dL) significantly decreased, according to our findings. This demonstrated the powerful anti-diabetic effects of those NPs. ZnO NPs, on the other hand, cause a decrease in blood glucose levels and are a powerful metal that enhances hepatic glycogenesis by acting on the insulin signaling system, thus improving glucose use and metabolism [88]. In addition to being essential for insulin production, secretion, and storage, zinc is also in charge of preserving the structure of insulin [89,90]. Studies have indicated that several zinc transporters, including zinc transporter-8, are essential for the secretion of insulin from

beta cells of the pancreas. Through several mechanisms, such as increased insulin receptor phosphorylation, increased phosphoinositide 3-kinase activity, and suppression of glycogen synthase kinase-3, ZnO NPs may also improve insulin signaling [91]. ZnO NPs can also reverse the effects of diabetes on pancreatic tissue. Diabetes-related pancreatic damage was restored by ZnO NPs, as demonstrated by structural and ultrastructural alterations, and confirmed by mean biochemical stability around blood sugar and serum insulin [92].

4.6 Role of ZnO NPs in induction of phagocytosis

In addition to circulating plasma proteins, the innate immune system is made up of basophils, mast cells, eosinophils, phagocytic cells (monocyte/macrophages, DCs, and polymorphonuclear leukocytes), physical epithelial barriers, and natural killer cells, sometimes referred to as complement and consistently found in body fluids such as tissues, lymph, and blood. The binding of opsonins triggers the innate immune system's rapid and non-specific reaction to any threat, eventually resulting in phagocytosis and clearance. Findings of the present study verify the ability of ZnO NPs to enhance treated BMDM cells to phagocytose and kill the bacteria. This experiment aimed to test how pre-treatment with ZnO NPs could stimulate the ability of BMDMs to phagocytose pHrodo E. coli bioparticles. We also aimed to test the mechanisms that could be involved in this process. Taken together, the results demonstrated that pre-treatment with ZnO NPs increases the ability to produce phagocytosis. This suggests that the ability of BMDMs to kill microorganisms could be enhanced. This experiment aimed to test how pretreatment with ZnO NPs could stimulate the ability of BMDMs in phagocytosis. We also aimed to test the mechanisms that could be involved in this process. Following internalization, NPs may go through several phagocyte processing stages. When endosomes or phagosomes internalize, they can combine with lysosomes to neutralize the NPs by lowering pH levels or by enzymatic digestion [93]; cell-free antimicrobial defense mechanisms since autophagy might exacerbate cell death through mitochondrial dysregulationand be harmful in the case of bio-persistent NPs [94]. However, harmful effects can be minimized if the cell can compartmentalize NPs into autophagosomes, separating them from additional interactions. This is advantageous for the cell as a stress-reduction strategy [94]. In the process of binding molecules and facilitating their absorption, the NP's curvature and size play a crucial role. Bigger NPs typically adsorb bigger proteins, including complement components

and immunoglobulins. For instance, opsonin C3b takes up about 40 nm² of space. Even tiny NPs do not provide enough space for binding [95]. Additionally, absorption processes vary according to the size of the particles. Smaller particles (less than 200 nm) are internalized through clathrin- or caveolar-mediated endocytosis, whereas bigger particles are more frequently taken up by phagocytosis, which is more impacted by opsonin adsorption [96]. Different NP kinds have distinct effects on the polarization and reprograming of macrophages [97]. The attention of the domains of nanotoxicology and other medical applications was drawn to the interaction between the NPs and these phagocytic cells in different states, as well as the other related nobodies [98]. To successfully modulate the in vivo biological effects of NPs and develop NP-based therapeutics and therapeutic regimes, a more profound comprehension of the functions these nanoscale particles play in macrophage polarization is necessary [99]. When ZnO NPs were added to the phagocytic cells, phagocytic cell activity was shown to significantly induce. ZnO NPs could induce or stimulate the ROS and NOX2 pathway to enhance phagocytosis activity. A reasonable explanation for the increased immune response and phagocytosis activity is likely due to the presence of immune-modulator entities that contribute to increased levels of phagocytic cells, as well as the presence of ZnO NPs that cause phagocytic cell maturation and involvement of the NOX2 pathway. This information could be used to improve antibacterial preparation and designs. Taken together, the current study also suggested that the chemical components of ZnO NPs may function as immunological enhancers, improving the activity of phagocytic cells to take up bacteria and other xenobiotics. Nevertheless, further studies are required to determine the precise chemical roles of the NPs.

4.7 Role of ZnO NPs in autophagy induction

The remarkable mechanical qualities, chemical stability, and biocompatibility of metallic NPs, one of the most thoroughly investigated biomaterials demonstrating autophagy induction, have garnered significant attention recently for potential uses in tissue regeneration. Because silver nanoparticles (AgNPs) have been shown to have antibacterial properties, they have proven helpful in clinical treatment. Autophagy has been shown to serve as a link between metallic NPs and wound healing. We hypothesized that once BMDM cells were pretreated with ZnO NPs following LPS and ATP, they would increase autophagy process markers. Using immunofluorescence tests, we investigated the

expression of LC3, a significant autophagy-related protein, to ascertain whether BMDMs treated with ZnO NPs trigger autophagy. Our findings showed that after treating LPS + ATP, BMDMs showed autophagy LC3 marker. In cells that had been pre-treated with ZnO NPs, the absolute amount of LC3 increased. AgNPs inhibited HO-1 and ROS formation in NIH-3T3 cells by upregulating LC3, which triggered autophagy and inhibited apoptosis [100]. By triggering autophagy and averting microbial infection, superparamagnetic iron oxide NPs dramatically reduced sepsis brought on by LPS [101]. Previous studies have been published on how NPs affect autophagy modulation. It had been thought that NP-induced autophagy served as a defense mechanism against toxicity generated by NMs as well as a mechanism of nontoxicity [102]. NPs are promising materials for initiating autophagy because of their inherent capacity to control the autophagy process at different stages. When lysosomes absorb and break down polymeric NPs, like poly(lactic-co-glycolic acid) NPs, there is an increase in acidity in the lysosomes, which causes an increase in autophagic flux and a decrease in SOSTM1/p62 [103]. ZnO NPs also cause autophagy flux, through inhibiting the MTOR signaling pathway or by causing the BCL2-family and autophagy-related proteins expressed [104]. Other studies demonstrated the ability of CuO, TiO₂, nitrogen-doped TiO₂, cerium dioxide, iron oxide, and neodymium (III) oxide (Nd₂O₃) NPs to increase autophagy flux by producing ROS or by employing other processes that significantly control lung, cervix, and breast cancer cell proliferation [105,106]. In summary, NMs have distinct impacts on wound regeneration and repair and induce autophagy through diverse signaling pathways. Consequently, studying autophagy triggered by NMs sheds light on skin wound healing while also clarifying the molecular mechanism of autophagy.

4.8 Docking study

GlcN-6-P synthase, referred to by the trivial name of L-Glutamine: D-fructose-6-phosphate amidotransferase, represents the active target of antibacterial chemotherapy. This enzyme plays a critical role in constructing bacterial cell walls through the biosynthesis of sugar-containing macromolecules. This enzyme catalyzes two reactions: first, it forms GlcN-6-P from D-fructose 6-phosphate (Fru-6-P); second, it forms uridine-5-diphospho-*N*-acetyl-D-glucosamine (UDP-GlcNAc), which is crucial for the building of bacterial cell walls [107]. ER alpha regulates neural, skeletal, cardiovascular, and reproductive tissue differentiation and maintenance. Compounds modulating ER alpha

transcriptional activity are currently used to treat osteoporosis, cardiovascular disease, and breast cancer. 4-Hydroxytamoxifen, the synthetic inhibitor for ER alpha, acts as a valuable agent for the treatment of breast cancer [108,109]. Tubulin is a dimeric protein comprising two subunits, α and β , that are related but not identical. Almost 30 years have passed since chalcones were initially identified as antimitotic agents [110]. Three active components of red radish, rutin, sinigrin, and dihydrocaffeic acid 3-O-glucuronide were modeled as colchicine analogs based on the knowledge of the structure-activity relationship between colchicine and tubulin. A rapid disruption of mitotic spindle assembly, interference with the cytoskeleton's function, and disrupted mitosis can be caused by colchicine analogs binding to tubulin and inhibiting its polymerization [111]. In silico docking explored the virtual affinity and the binding mode of the three active components extracted from the red radish inside three target macromolecules related to antimicrobial (GlcN-6-P synthase) and anticancer agents (Estrogen Receptor and Tubulin Receptor). The docking investigation revealed that the active compounds attach to the enzyme or protein's active site similar to the substrate or inhibitor. The results of the binding study confirmed this.

5 Conclusion

ZnO NPs are widely used in various biological applications due to their affordability, biocompatibility, and low toxicity. ZnO NPs have been shown to produce antibacterial and anticancer effects. Notably, synthesizing ZnO NPs from plant extracts is a good option against bacterial growth and proliferation of cancer cells. ZnO NP-mediated R. sativus (Red radish) exhibited anticancer activity against lung cancer cells through apoptosis proteins. The present study's findings demonstrated that ZnO NPs have anticancer, antibacterial, and antiviral effects. The molecular mechanisms demonstrated that ZnO NPs inhibit MDCK cell apoptosis by decreasing the level of ROS. Molecular docking studies the affinity within the target enzymes GlcN-6-P synthase (PDB:1MOQ) active site, Estrogen Receptor (PDB:3ERT) active site, and Tubulin Receptor (PDB:402B) active site. The results showed that the ZnO NPs have an inhibitory activity against pathogenic bacteria, inhibits proliferation of lung cancer cell lines, antiviral activity against influenza virus, and antidiabetic agent. Conversely, the results showed the ability of ZnO NPs to reduce inflammasome activity via augmented of autophagy. The docking investigation revealed that the active compounds attach to the enzyme or protein's

active site similar to the substrate or inhibitor. The results of the binding study confirmed this. Therefore, ZnO NPs mediated *R. sativus* have anticancer, antibacterial, and antiviral activities and could be a novel therapeutic strategy against cancer and associated viral and bacterial infections.

Funding information: The authors extend their appreciation to the Researchers Supporting Project number (RSPD2024R971), King Saud University, Riyadh, Saudi Arabia for funding this research.

Author contributions: All authors have accepted responsibility for the entire content of this manuscript and approved its submission.

Conflict of interest: The authors state no conflict of interest.

Ethical approval: The research related to animals' use has been complied with all the relevant national regulations and institutional policies for the care and use of animals.

Data availability statement: The datasets generated and/ or analyzed during the current study are available from the corresponding author on reasonable request.

References

- [1] Kirtane AR, Verma M, Karandikar P, Furin J, Langer R, Traverso G. Nanotechnology approaches for global infectious diseases. Nat Nanotechnol. 2021 Apr;16(4):369–84.
- [2] Kumhar BL. Concept and approaches of nano technology. Agric Mirror Future India. 2020;1(2):19–23.
- [3] Anselmo AC, Mitragotri S. Nanoparticles in the clinic: an update. Bioeng Transl Med. 2019 Sep;4(3):e10143.
- [4] El-Shafai N, El-Khouly ME, El-Kemary M, Ramadan M, Eldesoukey I, Masoud M. Graphene oxide decorated with zinc oxide nanoflower, silver and titanium dioxide nanoparticles: fabrication, characterization, DNA interaction, and antibacterial activity. RSC Adv. 2019;9(7):3704–14.
- [5] Gadewar M, Prashanth GK, Babu MR, Dileep MS, Prashanth PA, Rao S, et al. Unlocking nature's potential: Green synthesis of ZnO nanoparticles and their multifaceted applications-a concise overview. J Saudi Chem Soc. 2023;28:101774.
- [6] Eivazzadeh-Keihan R, Taheri-Ledari R, Khosropour N, Dalvand S, Maleki A, Mousavi-Khoshdel SM, et al. Fe₃O₄/GO@ melamine-ZnO nanocomposite: a promising versatile tool for organic catalysis and electrical capacitance. Colloids Surf A Physicochem Eng Asp. 2020 Feb;587:124335.
- [7] Haque MJ, Bellah MM, Hassan MR, Rahman S. Synthesis of ZnO nanoparticles by two different methods & comparison of their structural, antibacterial, photocatalytic and optical properties. Nano Express. 2020 Mar;1(1):010007.

- [8] Soto-Robles CA, Luque PA, Gómez-Gutiérrez CM, Nava O, Vilchis-Nestor AR, Lugo-Medina E, et al. Study on the effect of the concentration of *Hibiscus sabdariffa* extract on the green synthesis of ZnO nanoparticles. Results Phys. 2019 Dec 1;15:102807.
- [9] Hamdy MS, Chandekar KV, Shkir M, AlFaify S, Ibrahim EH, Ahmad Z, et al. Novel Mg@ ZnO nanoparticles synthesized by facile one-step combustion route for anti-microbial, cytotoxicity and photocatalysis applications. J Nanostruct Chem. 2021 Mar;11:147–63.
- [10] Hussain A, Oves M, Alajmi MF, Hussain I, Amir S, Ahmed J, et al. Biogenesis of ZnO nanoparticles using Pandanus odorifer leaf extract: anticancer and antimicrobial activities. RSC Adv. 2019;9(27):15357–69.
- [11] Islam F, Shohag S, Uddin MJ, Islam MR, Nafady MH, Akter A, et al. Exploring the journey of zinc oxide nanoparticles (ZnO-NPs) toward biomedical applications. Materials. 2022 Mar;15(6):2160.
- [12] Singh TA, Sharma A, Tejwan N, Ghosh N, Das J, Sil PC. A state of the art review on the synthesis, antibacterial, antioxidant, antidiabetic and tissue regeneration activities of zinc oxide nanoparticles. Adv Colloid Interface Sci. 2021 Sep;295:102495.
- [13] Ifijen IH, Maliki M, Anegbe B. Synthesis, photocatalytic degradation and antibacterial properties of selenium or silver doped zinc oxide nanoparticles: a detailed review. OpenNano. 2022 Sep;8:100082.
- [14] Wiesmann N, Tremel W, Brieger J. Zinc oxide nanoparticles for therapeutic purposes in cancer medicine. J Mater Chem B. 2020;8(23):4973–89.
- [15] Ren H, Zhao F, Zhang Q, Huang X, Wang Z. Autophagy and skin wound healing. Burn Trauma. 2022;10:tkac003. doi: 10.1093/ burnst/tkac003.
- [16] Pirot F, Kalia YN, Stinchcomb AL, Keating G, Bunge A, Guy RH. Characterization of the permeability barrier of human skin in vivo. Proc Natl Acad Sci U S A. 1997;94(4):1562–7. doi: 10.1073/pnas.94. 4.1562.
- [17] Lin JY, Lo KY, Sun YS. Effects of substrate-coating materials on the wound-healing process. Materials. 2019;12(17):2775. doi: 10.3390/ ma12172775.
- [18] Kim HS, Sun X, Lee JH, Kim HW, Fu X, Leong KW. Advanced drug delivery systems and artificial skin grafts for skin wound healing. Adv Drug Delivery Rev. 2019;146:209–39. doi: 10.1016/j.addr.2018. 12.014.
- [19] Birmingham CL, Smith AC, Bakowski MA, Yoshimori T, Brumell JH. Autophagy controls Salmonella infection in response to damage to the Salmonella-containing vacuole. J Biol Chem. 2006;281(16):11374–83. doi: 10.1074/jbc.M509157200.
- [20] Das LM, Binko AM, Traylor ZP, Peng H, Lu KQ. Vitamin D improves sunburns by increasing autophagy in M2 macrophages. Autophagy. 2019;15(5):813–26. doi: 10.1080/15548627.2019. 1569298.
- [21] Feng X, Zhang Y, Zhang C, Zhang C, Lai X, Zhang Y, et al. Nanomaterial-mediated autophagy: coexisting hazard and health benefits in biomedicine. Part Fibre Toxicol. 2020;17(1):53. doi: 10. 1186/s12989-020-00372-0.
- [22] Stern ST, Adiseshaiah PP, Crist RM. Autophagy and lysosomal dysfunction as emerging mechanisms of nanomaterial toxicity. Part Fibre Toxicol. 2012;9:20. doi: 10.1186/1743-8977-9-20.
- 23] Guo L, He N, Zhao Y, Liu T, Deng Y. Autophagy modulated by inorganic nanomaterials. Theranostics. 2020;10(7):3206–22. doi: 10.7150/thno.40414.

- [24] Chaudhari AA, Vig K, Baganizi DR, Sahu R, Dixit S, Dennis V, et al. Future prospects for scaffolding methods and biomaterials in skin tissue engineering: a review. Int J Mol Sci. 2016;17(12):E1974. doi: 10.3390/ijms17121974.
- [25] Berthet M, Gauthier Y, Lacroix C, Verrier B, Monge C. Nanoparticle-based dressing: the future of wound treatment? Trends Biotechnol. 2017;35:770–84.
- [26] Sharifi S, Hajipour MJ, Gould L, Mahmoudi M. Nanomedicine in healing chronic wounds: opportunities and challenges. Mol Pharm. 2021;18:550–75.
- [27] Raghupathi KR, Koodali RT, Manna AC. Size-dependent bacterial growth inhibition and mechanism of antibacterial activity of zinc oxide nanoparticles. Langmuir. 2011;27:4020–8.
- [28] Pati R, Mehta RK, Mohanty S, Padhi A, Sengupta M, Vaseeharan B, et al. Topical application of zinc oxide nanoparticles reduces bacterial skin infection in mice and exhibits antibacterial activity by inducing oxidative stress response and cell membrane disintegration in macrophages. Nanomed Nanotechnol Biol Med. 2014;10:1195–1208.
- [29] Rakhshaei R, Namazi H. A potential bioactive wound dressing based on carboxymethyl cellulose/ZnO impregnated MCM-41 nanocomposite hydrogel. Mater Sci Eng C. 2017;73:456–64.
- [30] Balaure PC, Holban AM, Grumezescu AM, Mogo,sanu GD, Băl,seanu TA, Stan MS, et al. In vitro and in vivo studies of novel fabricated bioactive dressings based on collagen and zinc oxide 3D scaffolds. Int | Pharm. 2019;557:199–207.
- [31] Shahzadi L, Chaudhry AA, Aleem AR, Malik MH, Ijaz K, Akhtar H, et al. Development of K-doped ZnO nanoparticles encapsulated crosslinked chitosan based new membranes to stimulate angiogenesis in tissue engineered skin grafts. Int J Biol Macromol. 2018;120:721–8.
- [32] Yang G, Zhang M, Qi B, Zhu Z, Yao J, Yuan X, et al. Nanoparticle-based strategies and approaches for the treatment of chronic wounds. J Biomater Tissue Eng. 2018;8:455–64.
- [33] Abbasi R, Shineh G, Mobaraki M, Doughty S, Tayebi L. Structural parameters of nanoparticles affecting their toxicity for biomedical applications: a review. J Nanopart Res. 2023;25(3):43. doi: 10.1007/ s11051-023-05690-w. Epub 2023 Feb 27. PMID: 36875184; PMCID: PMC9970140.
- [34] Khan FA. Nanomaterials: types, classifications, and sources. Applications of Nanomaterials in Human Health; 2020. p. 1–13.
- [35] Khan FA, Albalawi R, Pottoo FH. Trends in targeted delivery of nanomaterials in colon cancer diagnosis and treatment. Med Res Rev. 2022;42(1):227–58.
- [36] Rehman S, Almessiere MA, Khan FA, Korkmaz AD, Tashkandi N, Slimani Y, et al. Synthesis and biological characterization of Mn_{0.5}Zn_{0.5}Eu_xDy_xFe_{1.8-2x}O₄ nanoparticles by sonochemical approach. Mater Sci Eng C Mater Biol Appl. 2020 Apr;109:110534. doi: 10.1016/j.msec.2019.110534. Epub 2019 Dec 6. PMID: 32228890.
- [37] Nasimi P, Haidari M. Medical use of nanoparticles: drug delivery and diagnosis diseases. Int J Green Nanotechnol. 2013;1:1943089213506978. doi: 10.1177/1943089213506978.
- [38] Liu D, Liu L, Yao L, Peng X, Li Y, Jiang T, et al. Synthesis of ZnO nanoparticles using radish root extract for effective wound dressing agents for diabetic foot ulcers in nursing care. J Drug Delivery Sci Technol. 2020 Feb;55:101364.
- [39] Al Rugaie O, Jabir MS, Mohammed MK, Abbas RH, Ahmed DS, Sulaiman GM, et al. Modification of SWCNTs with hybrid materials ZnO-Ag and ZnO-Au for enhancing bactericidal activity of

- phagocytic cells against *Escherichia coli* through NOX2 pathway. Sci Rep. 2022;12(1):17203.
- [40] Rashid TM, Nayef UM, Jabir MS, Mutlak FA. Study of optical and morphological properties for Au-ZnO nanocomposite prepared by laser ablation in liquid. J Phys Conf Ser. 2021;1795(1):012041. IOP Publishing.
- [41] Mohammed SH, Singh S, Kadhum HH, Jabir MS. Adaption of MAPbI3 perovskite with copper phthalocyanine inorganic hole transport layer via nitrosonium tetrafluoroborate additive to enhance performance and stability of perovskite solar cells. Opt Mater. 2022;133:112901.
- [42] Sameen AM, Jabir MS, Al-Ani MQ. Therapeutic combination of gold nanoparticles and LPS as cytotoxic and apoptosis inducer in breast cancer cells. AIP Conf Proc. 2020;2213(1):020215. AIP Publishing.
- [43] Jasim AJ, Sulaiman GM, Ay H, Mohammed SA, Mohammed HA, Jabir MS, et al. Preliminary trials of the gold nanoparticles conjugated chrysin: an assessment of anti-oxidant, anti-microbial, and in vitro cytotoxic activities of a nanoformulated flavonoid. Nanotechnol Rev. 2022;11(1):2726–41.
- [44] Abbas ZS, Sulaiman GM, Jabir MS, Mohammed SA, Khan RA, Mohammed HA, et al. Galangin/β-cyclodextrin inclusion complex as a drug-delivery system for improved solubility and biocompatibility in breast cancer treatment. Molecules. 2022;27(14):4521.
- [45] Solanki R, Rajput PK, Jodha B, Yadav UC, Patel S. Enhancing apoptosis-mediated anticancer activity of evodiamine through protein-based nanoparticles in breast cancer cells. Sci Rep. 2024;14(1):2595.
- [46] Sylvester JT, Karnati SK, Yu Z, Morrison M, Firkins JL. Development of an assay to quantify rumen ciliate protozoal biomass in cows using real-time PCR. J Nutr. 2004;134(12):3378–84.
- [47] Palau M, Muñoz E, Gusta MF, Larrosa N, Gomis X, Gilabert J, et al. In vitro antibacterial activity of silver nanoparticles conjugated with amikacin and combined with hyperthermia against drugresistant and biofilm-producing strains. Microbiol Spectr. 2023;11(3):e00280–23.
- [48] Khashan KS, Badr BA, Sulaiman GM, Jabir MS, Hussain SA. Antibacterial activity of Zinc Oxide nanostructured materials synthesis by laser ablation method. J Phys Conf Ser. 2021;1795(1):012040. IOP Publishing.
- [49] Kadhim RJ, Karsh EH, Taqi ZJ, Jabir MS. Biocompatibility of gold nanoparticles: In vitro and In vivo study. Mater Today Proc. 2021;42:3041–5.
- [50] Al Awadh AA, Shet AR, Patil LR, Shaikh IA, Alshahrani MM, Nadaf R, et al. Sustainable synthesis and characterization of zinc oxide nanoparticles using *Raphanus sativus* extract and its biomedical applications. Crystals. 2022 Aug;12(8):1142.
- [51] Namvar F, Rahman HS, Mohamad R, Azizi S, Tahir PM, Chartrand MS, et al. Cytotoxic effects of biosynthesized zinc oxide nanoparticles on murine cell lines. Evid Based Complement Alternat Med. 2015;2015(1):593014.
- [52] Gilbert B, Fakra SC, Xia T, Pokhrel S, M\u00e4dler L, Nel AE. The fate of ZnO nanoparticles administered to human bronchial epithelial cells. ACS Nano. 2012 Jun;6(6):4921–30.
- [53] Gilbert B, Fakra SC, Xia T, Pokhrel S, M\u00e4dler L, Nel AE. The fate of ZnO nanoparticles administered to human bronchial epithelial cells. ACS Nano. 2012 Jun;6(6):4921–30.
- [54] Köerich JS, Nogueira DJ, Vaz VP, Simioni C, Silva ML, Ouriques LC, et al. Toxicity of binary mixtures of Al_2O_3 and ZnO nanoparticles

- toward fibroblast and bronchial epithelium cells. J Toxicol Environ Health Part A. 2020 May;83(9):363-77.
- [55] Giovanni M, Yue J, Zhang L, Xie J, Ong CN, Leong DT. Proinflammatory responses of RAW264. 7 macrophages when treated with ultralow concentrations of silver, titanium dioxide, and zinc oxide nanoparticles. J Hazard Mater. 2015 Oct;297:146-52.
- Di Giampaolo L, Zaccariello G, Benedetti A, Vecchiotti G, [56] Caposano F, Sabbioni E, et al. Genotoxicity and immunotoxicity of titanium dioxide-embedded mesoporous silica nanoparticles (TiO₂@ MSN) in primary peripheral human blood mononuclear cells (PBMC). Nanomaterials. 2021 Jan;11(2):270.
- Yin H, Casey PS, McCall MJ, Fenech M. Effects of surface chemistry on cytotoxicity, genotoxicity, and the generation of reactive oxygen species induced by ZnO nanoparticles. Langmuir. 2010 Oct;26(19):15399-408.
- [58] Kiliç G, Costa C, Fernández-Bertólez N, Pásaro E, Teixeira JP, Laffon B, et al. In vitro toxicity evaluation of silica-coated iron oxide nanoparticles in human SHSY5Y neuronal cells. Toxicol Res. 2016;5(1):235-47.
- Khan MJ, Ahmad A, Khan MA, Siddiqui S. Zinc oxide nanoparticle [59] induces apoptosis in human epidermoid carcinoma cells through reactive oxygen species and DNA degradation. Biol Trace Elem Res. 2021 Jun;199:2172-81.
- [60] Yang D, Zhang M, Gan Y, Yang S, Wang J, Yu M, et al. Involvement of oxidative stress in ZnO NPs-induced apoptosis and autophagy of mouse GC-1 spg cells. Ecotoxicol Environ Saf. 2020 Oct 1;202:110960.
- [61] Chen L, Wu H, Hong W, Aguilar ZP, Fu F, Xu H. The effect of reproductive toxicity induced by ZnO NPs in mice during early pregnancy through mitochondrial apoptotic pathway. Environ Toxicol. 2021 Jun;36(6):1143-51.
- Dawood L, Tousson E, El-Atrsh A, Salama A. Anti-proliferative effect of ZnO NPs against the growth of ehrlich solid carcinoma. J Med Life Sci. 2019 Dec 15;1(4):110-22.
- Perumal P, Sathakkathulla NA, Kumaran K, Ravikumar R, Selvaraj JJ, Nagendran V, et al. Green synthesis of zinc oxide nanoparticles using aqueous extract of shilajit and their anticancer activity against HeLa cells. Sci Rep. 2024;14:2204. doi: 10. 1038/s41598-024-52217-x.
- Voloshina M, Rajput VD, Minkina T, Vechkanov E, Mandzhieva S, Mazarji M, et al. Zinc oxide nanoparticles: physiological and biochemical responses in Barley (Hordeum vulgare L.). Plants (Basel). 2022 Oct;11(20):2759. doi: 10.3390/plants11202759. PMID: 36297783; PMCID: PMC9607964.
- Jena AB, Samal RR, Bhol NK, Duttaroy AK. Cellular red-ox system in health and disease: the latest update. Biomed Pharmacother. 2023;162:114606.
- [66] Jomova K, Alomar SY, Alwasel SH, Nepovimova E, Kuca K, Valko M, et al. Several lines of antioxidant defense against oxidative stress: antioxidant enzymes, nanomaterials with multiple enzymemimicking activities, and low-molecular-weight antioxidants. Arch Toxicol. 2024;98:1323-67. doi: 10.1007/s00204-024-03696-4.
- Sun J, Yu J, Niu X, Zhang X, Zhou L, Liu X, et al. Solid fuel derived PM2.5 induced oxidative stress and according cytotoxicity in A549 cells: the evidence and potential neutralization by green tea. Environ Int. 2023;171:107674.
- Barzgar F, Sadeghi-Mohammadi S, Aftabi Y, Zarredar H, Shakerkhatibi M, Sarbakhsh P, et al. Oxidative stress indices

- induced by industrial and urban PM2.5-bound metals in A549 cells. Sci Total Environ. 2023;877:162726.
- [69] Hayes JD, Dinkova-Kostova AT, Tew KD. Oxidative stress in cancer. Cancer Cell. 2020 Aug;38(2):167-97.
- [70] Arfin S, Jha NK, Jha SK, Kesari KK, Ruokolainen J, Roychoudhury S, et al. Oxidative stress in cancer cell metabolism. Antioxidants. 2021 Apr;10(5):642.
- [71] Azmanova M, Pitto-Barry A. Oxidative stress in cancer therapy: friend or enemy? Chembiochem. 2022 May;23(10):e202100641.
- [72] Dutta RK, Nenavathu BP, Gangishetty MK, Reddy AV. Studies on antibacterial activity of ZnO nanoparticles by ROS induced lipid peroxidation. Colloids Surf B Biointerfaces. 2012 Jun;94:143-50.
- [73] da Silva BL, Caetano BL, Chiari-Andréo BG, Pietro RC, Chiavacci LA. Increased antibacterial activity of ZnO nanoparticles: Influence of size and surface modification. Colloids Surf B Biointerfaces. 2019 May;177:440-7.
- Dutta RK, Nenavathu BP, Gangishetty MK, Reddy AV. Antibacterial effect of chronic exposure of low concentration ZnO nanoparticles on E. coli. J Environ Sci Health Part A. 2013 Jul;48(8):871-8.
- [75] Romadhan MF, Suyatma NE, Tagi FM. Synthesis of ZnO nanoparticles by precipitation method with their antibacterial effect. Indonesian J Chem. 2016 Jul;16(2):117-23.
- Jiang Y, Zhang L, Wen D, Ding Y. Role of physical and chemical [76] interactions in the antibacterial behavior of ZnO nanoparticles against E. coli. Mater Sci Eng C. 2016 Dec;69:1361-6.
- Zhang L, Jiang Y, Ding P, Povey M, York D. Investigation into the [77] antibacterial behavior of suspensions of ZnO nanoparticles (ZnO nanofluids). J Nanopart Res. 2007;9:479-89.
- [78] Naskar A, Lee S, Kim KS. Antibacterial potential of Ni-doped zinc oxide nanostructure: comparatively more effective against Gramnegative bacteria including multi-drug resistant strains. RSC Adv. 2020;10(3):1232-42.
- [79] Melk MM, El-Hawary SS, Melek FR, Saleh DO, Ali OM, El Raey MA, et al. Antiviral activity of zinc oxide nanoparticles mediated by Plumbago indica L. Extract against herpes simplex virus type 1 (HSV-1). Int J Nanomed. 2021;16:8221.
- [80] Attia GH, Moemen YS, Youns M, Ibrahim AM, Abdou R, El Raey MA. Antiviral zinc oxide nanoparticles mediated by hesperidin and in silico comparison study between antiviral phenolics as anti-SARS-CoV-2. Colloids Surf B Biointerfaces. 2021 Iul:203:111724.
- [81] Shehabeldine AM, Hashem AH, Wassel AR, Hasanin M. Antimicrobial and antiviral activities of durable cotton fabrics treated with nanocomposite based on zinc oxide nanoparticles, acyclovir, nanochitosan, and clove oil. Appl Biochem Biotechnol. 2022 Feb;194:1-8.
- [82] Ghaffari H, Tavakoli A, Moradi A, Tabarraei A, Bokharaei-Salim F, Zahmatkeshan M, et al. Inhibition of H1N1 influenza virus infection by zinc oxide nanoparticles: another emerging application of nanomedicine. J Biomed Sci. 2019 Dec;26(1):1.
- [83] Siddiqi KS, ur Rahman A, Husen A. Properties of zinc oxide nanoparticles and their activity against microbes. Nanoscale Res Lett. 2018:13(1):141.
- Kumar R, Sahoo G, Pandey K, Nayak MK, Topno R, Rabidas V, et al. [84] Virostatic potential of zinc oxide (ZnO) nanoparticles on capsid protein of cytoplasmic side of chikungunya virus. Int J Infect Dis.
- [85] Kar B, Pradhan D, Mishra P, Bhuyan SK, Ghosh G, Rath G. Exploring the potential of metal nanoparticles as a possible

- therapeutic adjunct for covid-19 infection. Proc Natl Acad Sci, India Sect B Biol Sci. 2022 Sep;92(3):511–21.
- [86] Nagaich U, Gulati N, Chauhan S. Antioxidant and antibacterial potential of silver nanoparticles: biogenic synthesis utilizing apple extract. J Pharm. 2016;2016:1–8.
- [87] Siripireddy B, Mandal BK. Facile green synthesis of zinc oxide nanoparticles by Eucalyptus globulus and their photocatalytic and antioxidant activity. Adv Powder Technol. 2017;28:785–97.
- [88] Jansen J, Karges W, Rink L. Zinc and diabetes—clinical links and molecular mechanisms. J Nutr Biochem. 2009;20:399–417.
- [89] Nazarizadeh A, Asri-Rezaie S. Comparative study of antidiabetic activity and oxidative stress induced by zinc oxide nanoparticles and zinc sulfate in diabetic rats. AAPS Pharm Sci Tech. 2016;17:834–43.
- [90] Umrani RD, Paknikar KM. Zinc oxide nanoparticles show antidiabetic activity in streptozotocin-induced type 1 and 2 diabetic rats. Nanomedicine. 2014;9:89–104.
- [91] Siddiqui SA, Rashid MMO, Uddin MG, Robel FN, Hossain MS, Haque MA, et al. Biological efficacy of zinc oxide nanoparticles against diabetes: a preliminary study conducted in mice. Biosci Rep. 2020;40:1–8.
- [92] Wahba NS, Shaban SF, Kattaia AAA, Kandeel SA. Efficacy of zinc oxide nanoparticles in attenuating pancreatic damage in a rat model of streptozotocin-induced diabetes. Ultrastruct Pathol. 2016;40:358–73.
- [93] Zaki NM, Tirelli N. Gateways for the intracellular access of nanocarriers: a review of receptor-mediated endocytosis mechanisms and of strategies in receptor targeting. Expert Opin Drug Deliv. 2010;7(8):895–913. doi: 10.1517/17425247.2010.501792.
- [94] Stern ST, Adiseshaiah PP, Crist RM. Autophagy and lysosomal dysfunction as emerging mechanisms of nanomaterial toxicity. Part Fibre Toxicol. 2012;9(1):1–17. doi: 10.1186/1743-8977-9-20.
- [95] Papini E, Tavano R, Mancin F. Opsonins and dysopsonins of nanoparticles: facts, concepts, and methodological guidelines. Front Immunol. 2020;11:567365. doi: 10.3389/fimmu.2020. 567365
- [96] Oyewumi MO, Kumar A, Cui Z. Nano-microparticles as immune adjuvants: correlating particle sizes and the resultant immune responses. Expert Rev Vaccines. 2010;9(9):1095–107. doi: 10.1586/ erv.10.89.
- [97] Fuchs AK, Syrovets T, Haas KA, Loos C, Musyanovych A, Mailänder V, et al. Carboxyl-and amino-functionalized polystyrene nanoparticles differentially affect the polarization profile of M1 and M2 macrophage subsets. Biomaterials. 2016;85:78–87.
- [98] Talekar M, Tran TH, Amiji M. Translational nano-medicines: targeted therapeutic delivery for cancer and inflammatory diseases. AAPS J. 2015;17:813–27.
- [99] Peng J, Liang X. Progress in research on gold nanoparticles in cancer management. Medicine. 2019;98(18):e15311.

- [100] Lee YH, Cheng FY, Chiu HW, Tsai J-C, Fang C-Y, Chen C-W, et al. Cytotoxicity, oxidative stress, apoptosis and the autophagic effects of silver nanoparticles in mouse embryonic fibroblasts. Biomaterials. 2014;35(16):4706–15. doi: 10.1016/j.biomaterials. 2014.02.021.
- [101] Xu Y, Li Y, Liu X, Pan Y, Sun Z, Xue Y, et al. SPIONs enhances IL-10-producing macrophages to relieve sepsis via Cav1-Notch1/HES1-mediated autophagy. Int J Nanomed. 2019;14:6779–97. doi: 10. 2147/IIN.S215055.
- [102] Chen RJ, Chen YY, Liao MY, Lee YH, Chen ZY, Yan SJ, et al. The current understanding of autophagy in nanomaterial toxicity and its implementation in safety assessment-related alternative testing strategies. Int J Mol Sci. 2020;21(7):2387.
- [103] Trudeau KM, Colby AH, Zeng J, Las G, Feng JH, Grinstaff MW, et al. Lysosome acidification by photoactivated nanoparticles restores autophagy under lipotoxicity. J Cell Biol. 2016;214(1):25–34.
- [104] Roy R, Singh SK, Chauhan LKS, Das M, Tripathi A, Dwivedi PD. Zinc oxide nanoparticles induce apoptosis by enhancement of autophaqy via PI3K/Akt/mTOR inhibition. Toxicol Lett. 2014;227(1):29–40.
- [105] Zhang X, Zhang H, Liang X, Zhang J, Tao W, Zhu X, et al. Iron oxide nanoparticles induce autophagosome accumulation through multiple mechanisms: lysosome impairment, mitochondrial damage, and ER stress. Mol Pharmaceutics. 2016;13(7):2578–87.
- [106] Xia L, Wang Y, Chen Y, Yan J, Hao F, Su X, et al. Cuprous oxide nanoparticles inhibit the growth of cervical carcinoma by inducing autophagy. Oncotarget. 2017;8(37):61083.
- [107] Bearne SL, Blouin C. Inhibition of Escherichia coli Glucosamine-6phosphate Synthase by reactive intermediate analogues: The role of the 2-amino function in catalysis. J Biol Chem. 2000;275(1):135–40. doi: 10.1074/jbc.275.1.135.
- [108] Naidu CK, Suneetha Y. Molecular docking, QSAR and AMDET analysis of 6-methyl-1,3,8-trichlorodibenzofuran and its analogs against Estrogen receptor alpha. Med Chem Res. 2014;23:4724–48. doi: 10.1007/s00044-014-1039-4.
- [109] Bai C, Ren S, Wu S, Zhu M, Luo G, Xiang H. Design and synthesis of novel benzothiophene analogs as selective estrogen receptor covalent antagonists against breast cancer. Eur J Med Chem. 2021 Oct;221:113543. doi: 10.1016/j.ejmech.2021.113543. Epub 2021 May 14. PMID: 34022716.
- [110] Arnst KE, Banerjee S, Chen H, Deng S, Hwang DJ, Li W, et al. Current advances of tubulin inhibitors as dual acting small molecules for cancer therapy. Med Res Rev. 2019 Jul;39(4):1398–426. doi: 10.1002/med.21568, Epub 2019 Feb 11. PMID: 30746734; PMCID: PMC6857175.
- [111] Boichuk S, Syuzov K, Bikinieva F, Galembikova A, Zykova S, Gankova K, et al. Computational-based discovery of the anticancer activities of pyrrole-based compounds targeting the colchicine-binding site of tubulin. Molecules. 2022;27:2873. doi: 10. 3390/molecules27092873.